

Design and synthesis of novel pyrazole-phenyl semicarbazone derivatives as potential α -glucosidase inhibitor: Kinetics and molecular dynamics simulation study

Fateme Azimi, Jahan B. Ghasemi, Homa Azizian, Mohammad Najafi, Mohammad Ali Faramarzi, Lotfollah Saghaei, Hojjat Sadeghi-aliabadi, Bagher Larijani, Farshid Hassanzadeh, Mohammad Mahdavi



PII: S0141-8130(20)34916-3

DOI: <https://doi.org/10.1016/j.ijbiomac.2020.10.263>

Reference: BIOMAC 17153

To appear in: *International Journal of Biological Macromolecules*

Received date: 25 September 2020

Revised date: 29 October 2020

Accepted date: 31 October 2020

Please cite this article as: F. Azimi, J.B. Ghasemi, H. Azizian, et al., Design and synthesis of novel pyrazole-phenyl semicarbazone derivatives as potential α -glucosidase inhibitor: Kinetics and molecular dynamics simulation study, *International Journal of Biological Macromolecules* (2018), <https://doi.org/10.1016/j.ijbiomac.2020.10.263>

This is a PDF file of an article that has undergone enhancements after acceptance, such as the addition of a cover page and metadata, and formatting for readability, but it is not yet the definitive version of record. This version will undergo additional copyediting, typesetting and review before it is published in its final form, but we are providing this version to give early visibility of the article. Please note that, during the production process, errors may be discovered which could affect the content, and all legal disclaimers that apply to the journal pertain.

Design and synthesis of novel pyrazole-phenyl semicarbazone derivatives as potential α -glucosidase inhibitor: Kinetics and molecular dynamics simulation study

Fateme Azimi ^a, Jahan B. Ghasemi ^b, Homa Azizian ^c, Mohammad Najafi ^d, Mohammad Ali Faramarzi ^e, Lotfollah Saghaei ^{a,*1}, Hojjat Sadeghi-aliabadi ^a, Bagher Larijani ^f, Farshid Hassanzadeh ^{a,*}, Mohammad Mahdavi ^{f,*}

^a Department of Medicinal Chemistry, Faculty of Pharmacy, Isfahan University of Medical Sciences, Isfahan, Iran

^b Department of Chemistry, Faculty of Sciences, University of Tehran, Tehran, Iran

^c Department of Medicinal Chemistry, School of Pharmacy-International Campus, Iran University of Medical Science, Tehran, Iran

^d Department of Chemistry, Isfahan University of Technology, Isfahan, Iran

^e Department of Pharmaceutical Biotechnology, Faculty of Pharmacy and Biotechnology Research Center, Tehran University of Medical Sciences, Tehran, Iran

^f Endocrinology and Metabolism Research Center, Endocrinology and Metabolism Research Institute, Tehran University of Medical Sciences, Tehran, Iran

Abstract

A series of novel pyrazole-phenyl semicarbazone derivatives were designed, synthesized, and screened for *in vitro* α -glucosidase inhibitory activity. Given the importance of hydrogen bonding in promoting the α -glucosidase inhibitory activity, pharmacophore modification was established. The docking results rationalized the idea of the design. All newly synthesized compounds exhibited excellent *in vitro* yeast α -glucosidase inhibition (IC_{50} values in the range of 65.1 - 695.0 μ M) even much more potent than standard drug acarbose ($IC_{50}=750.0$ μ M). Among them, compounds 8o displayed the most potent α -glucosidase inhibitory activity ($IC_{50} = 65.1 \pm 0.3$ μ M). Kinetic study of compound 8o revealed that it inhibited α -glucosidase in a competitive mode ($K_i = 87.0$ μ M). Limited SAR suggested that electronic properties of substitutions have little effect on inhibitory potential of compounds. Cytotoxic studies demonstrated that the active compounds (8o, 8k, 8p, 8l, 8i, and 8a) compounds are also non-cytotoxic. The binding modes of the most potent compounds 8o, 8k, 8p, 8l and 8i was studied through *in silico* docking studies. Molecular dynamic simulations have been performed in order to explain the dynamic behavior

* Corresponding authors.

E-mail addresses: saghaei@pharm.mui.ac.ir (L. Saghaie), hassanzadeh@pharm.mui.ac.ir (F. Hassanzadeh), momahdavi@tums.ac.ir (M. Mahdavi)

and structural changes of the systems by the calculation of the root mean square deviation (RMSD) and root mean square fluctuation (RMSF).

Keywords:

α -Glucosidase inhibitor; Synthesis; Pyrezole; Structure–activity relationship; Enzyme kinetic study; Molecular dynamic simulation

1. Introduction

Diabetes mellitus (DM) is a chronic metabolic disorder resulting from defects in insulin action (type 2 diabetes), insulin secretion (type 1 diabetes), or both, which affects the metabolic functions of the endocrine system. Diabetes is undoubtedly one of the major public health problems worldwide [1, 2]. According to WHO reports, more than 420 million people are suffering from diabetes and this number is expected to be more than 642 million by 2040 [2, 3]. Type-2 diabetes is the most common type and accounts for approximately 80-90% of all diabetic cases, which is responsible for around 5% death globally [4-6]. This dysfunction leads to high blood glucose concentration or hyperglycemia. Prolonged hyperglycemia causes a wide variety of critical complications, including diabetic neuropathy [7, 8], cancer [9, 10], retinopathy [11], stroke [12, 13], amputations [14, 15], microangiopathy, and cardiovascular diseases [16-18].

One of the critical strategies to control diabetes complications is by managing the blood glucose level [19]. α -Glucosidase inhibitors prevent the hydrolysis α -glucosidic bond of complex carbohydrates and delay monosaccharide (α -D-glucose) absorption, which is mainly responsible to cause hyperglycemia [20]. Thus, α -glucosidase inhibitors have been considered as a most attractive therapeutic target for drug discovery in the treatment of type 2 diabetes [21-23]. Beside, α -glucosidase is biocatalyst involved in a series of relevant processes like glycolipid and glycoprotein metabolic routes, cell-to-cell signaling, and virus recognition [24, 25]. Therefore, glucosidase inhibitors have attracted plenty of interest by the pharmaceutical industry as novel agents to treat other carbohydrate mediated diseases including viral infections, hepatitis, cancer, pompe disease, and other degenerative diseases such as nojirimycin and castanospermine [25-30]. Currently, glycosidic based α -glucosidase inhibitors such as acarbose (Glucobay), miglitol (Glyset), and voglibose (Volix, Basen) are clinically used in the treatment of type-2 diabetes

mellitus [31]. Although these medications have a certain therapeutic effect on diabetes, they are associated with serious adverse. As the result, they have to be used in combination with other anti-diabetic agents to improve the effectiveness [32]. On the other hand, the synthesis of other similar derivatives of mentioned α -glucosidase inhibitors is tedious and need complicated multi-step procedures due to the presence of sugar moieties in their structures [33]. So, it is still an appealing and interesting area of medicinal chemistry research to discovery and develop efficient small molecules capable of possessing potent α -glucosidase inhibitory activities.

The heterocyclic scaffolds have attracted considerable attention of medicinal chemists due to their exceptional chemical and versatile biological profiles. In this category, pyrazole and their derivatives represent one of the key structural units in numerous medicinally important compounds with various pharmacological effects including anti-inflammatory, analgesic, antimicrobial, neuroprotective, antihypercholesterolemia, antimalarial, anti-Alzheimer, antihypertensive, antitubercular, antiviral, and antihyperglycaemic activities [34-36]. Pyrazole scaffold has also reported to show selective and potent inhibitory activity against lung, colon, renal, prostate, and breast cancer cells [37, 38]. Furthermore, pyrazole derivatives possess the LRRK2 inhibitory activity to identify new drugs to treat Parkinson's disease [39]. Several pyrazole containing drug molecules with diverse therapeutic activities such as Celecoxib, sildenafil, Crizotinib, Surinabant, Pimobendan, and Pyrazofurin are now available in the market [34]. Historically, different substituted pyrazole had been reported as in vivo anti hypoglycemic agent [40]. Also, recent studies have confirmed that several entities of the pyrazole have been possessed antidiabetic [41-43] and hypoglycemic [44-46] activity (Fig. 1). In addition to the mentioned successful studies, significant metabolic stability and pharmacological efficiency of pyrazole derivatives as antidiabetic agents and approved the "Teneligliptin", a pyrazole motif containing antidiabetic drug, encouraged us to further study on pyrazole scaffolds[47].

Benzohydrazides are important classes of compounds due to its wide range of activities, including antiglycation, antioxidant, antileishmanial, antitumor, antibacterial, and anticonvulsant [48-53]. In recent years, several compounds possessing benzohydrazide scaffolds with high α -glucosidase inhibitory activity have been reported [25, 54]. for instance, benzothiazole hybrids having benzohydrazide moiety (Fig. 2 compound C) were reported by Taha et al. as a potent α -glucosidase inhibitor ($IC_{50} = 5.31 \pm 0.03 \mu M$ comparing with acarbose, $906 \pm 6.3 \mu M$) [54].

Molecular hybridization has been a strong tool to design and develop new biologically active compounds with improved potency. In this work, in continuation of our efforts for developing new α -glucosidase inhibitors using molecular hybridization and endeavoring to extend the chemical space, we designed a new scaffold in order to identify lead candidates for more advanced research in future [55-57]. Steps for the rational design of new hybrid are depicted in Fig. 3. Enormous importance of hydrogen bonding in promoting the α -glucosidase inhibitory activity has inspired the modification of benzohydrazide to the phenyl semicarbazide moiety, which introduced extra nitrogen atom into the structure as hydrogen bond donor (Fig. 2 compound D). Modifications were implemented in the designed hybrid in order to enhance the key factors required to promote the glucosidase inhibitory such as π -stacking, hydrogen bonding, and hydrophobicity [58, 59]. Hydrazone linker was included in the design of the new hybrid as part of the initial design. It was hypothesized that the addition of the hydrazone linkage could substantially decrease the entropic penalty for the formation of the enzyme-inhibitor complex (Fig. 2 compound B) [25]. Accordingly, our research team designed and synthesized a new hybrid moiety that incorporated pyrazole, phenyl semicarbazide, and hydrazone in a single structural entity and evaluated them against α -glucosidase enzyme for the first time. The docking results rationalized the idea of conjugation of pyrazole with arylsemicarbazone moiety. The designed hybrid packed in the catalytic hydrophobic pocket of active site whereas nitrogen and oxygen atoms of the semicarbazide formed hydrogen bonds with the enzyme (Fig. 2E).

Apart from *in vitro* assessment of target compounds, *in silico* study and mechanism underlying enzymatic inhibition were also investigated to have a better understanding of the interactions of the title compounds with α -glucosidase. Moreover, molecular dynamic simulation was performed to explain of the dynamic behavior and structural changes of the system.

Please insert Fig. 1 about here

Please insert Fig. 2 about here

2. Result and discussion

2.1. Chemistry

The pathway for the synthesis of pyrazole-phenyl semicarbazone hybrids 8a-p has been depicted in Scheme 1. Different substituted acetophenones 1 reacted with phenyl hydrazine or 4-methyl phenyl hydrazine 2 in the presence of sulfuric acid in absolute ethanol to afford the hydrazone intermediates 3a-p. The synthesized hydrazone intermediates 3a-p then undergo a Vilsmeier–Hack reaction in the presence of DMF and POCl₃ to form pyrazole carbaldehydes 4a-p. On the other hand, 4-phenyl semicarbazide 7 was constructed according to the known urea preparation method [60]. Aniline 5 was treated with sodium cyanate in the presence of glacial acetic acid to yield phenyl urea 6. The 4-phenyl semicarbazide 7 was obtained upon refluxing phenyl urea 6 with hydrazine hydrate in ethanol in the presence of sodium hydroxide. Finally, pyrazole-phenyl semicarbazone hybrids 8a-p were synthesized by condensing equimolar amounts of 4-phenyl semicarbazide with different aldehydes in the presence of catalytic amount of acetic acid [61, 62].

Please insert Scheme 1 about here

2.2. *In vitro* α -glucosidase inhibitory activity and structure–activity relationships (SAR) study

All synthesized new hybrids 8a-p were screened for their *in vitro* α -glucosidase inhibitory potential. The IC₅₀ values were determined and acarbose as marketed α -glucosidase inhibitor was used for comparison purpose. In order to optimize the anti- α -glucosidase activity and better understanding of structure–activity relationship, substituent acetophenone, phenylhydrazine, and 4-methyl phenylhydrazine were used to synthesize various derivatives of the designed scaffold. The *in vitro* α -glucosidase inhibitory activity of tested compounds as IC₅₀ values are summarized in Table 1. Obtained results revealed that all the target compounds had excellent inhibitory activity in the range of IC₅₀ = 65.1 \pm 0.3 - 695.0 \pm 9.5 μ M and all of them were more potent than acarbose (IC₅₀ = 750.0 \pm 10.0 μ M). High inhibitory potential of designed compound suggested that all structural features such as pyrazole core, hydrazone linkage, and semicarbazide moiety are cordially playing their part in demonstrating the inhibitory potential; however, the variation of the substituents in the phenyl rings on the pyrazole moiety is responsible for variation in the inhibitory activity. Based on substituents in R₂, synthesized compounds can be categorized into two categories and SAR was interpreted based on substitution in R₁ in each series (Table 1).

Compound 8a-8i of “Category A” ($IC_{50} = 92.0 \pm 0.7$ - $695.0 \pm 9.5 \mu\text{M}$), having no substitution on R_2 . In this category, compound 8i ($IC_{50} = 92.0 \pm 0.7 \mu\text{M}$) with para trifluoromethyl substitution was found to be the most active compound with more than eight-fold higher activity than acarbose. Removal of trifluoromethyl group of compound 8i was associated with a slight decrease in activity as observed in the second most active analog in this series 8a ($IC_{50} = 96.3 \pm 0.8 \mu\text{M}$), whereas replacement of this group with other substituents (8b-8h), resulted in a moderate to significant decrease in the inhibitory activity in the range of $IC_{50}=157.3 \pm 1.9$ - $695.0 \pm 9.5 \mu\text{M}$. Despite the decrease in the activity of remaining compounds, their inhibitory potential was around 1–7 fold more than acarbose. Therefore, the activity pattern showed that other groups are less participating in the activity compared to the trifluoromethyl group. Interestingly, compounds 8f ($IC_{50} = 130.7 \pm 1.5 \mu\text{M}$) and 8g ($IC_{50} = 134.5 \pm 1.6 \mu\text{M}$) with nitro (electron withdrawing) and hydroxyl (electron donating) substituents on the para position of phenyl, respectively, showed almost similar inhibitory activity against α -glucosidase. These compounds were found to be the third most active in this category and it seemed that the electronic properties of substitutions did not have substantial effect on inhibitory potential. Replacing hydroxyl with methyl also decreased activity in compound 8b ($IC_{50} = 157.3 \pm 1.9 \mu\text{M}$), while methylation of the hydroxyl group in compound 8g further decreased the activity as observed in compound 8c ($IC_{50} = 182.6 \pm 2.5 \mu\text{M}$). Halogenated derivatives also displayed variable inhibition against α -glucosidase. By substitution of Cl or Br at the para positions (compounds 8d and 8e), identical inhibitory potential was observed, however, lower than compound 8i with CF_3 substitution. Replacement of Cl or Br by F resulted in a significant deterioration in activity in compound 8h. As a result, the IC_{50} value of compound 8c reached $695.0 \pm 9.5 \mu\text{M}$, which was more than four-fold lower than 8d or 8e. The interesting point about halogenated compounds was that 4- CF_3 derivative was the most potent analog, whereas 4-fluoro derivative was the least active molecule of all halo-substituted compounds. These results suggested that the inhibitory activity of halogenated compounds may be affected by the size of substitution. Compounds 8j-8p belong to Category-B having methyl group as R_2 showed their inhibitory activity in the range of $IC_{50} = 65.1 \pm 0.3$ - $506.2 \pm 8.5 \mu\text{M}$. In this group, compound 8o with a 4-nitro substituent showed the most inhibitory activity ($IC_{50} = 65.1 \pm 0.3 \mu\text{M}$), which was approximately 12 times more potent than acarbose ($IC_{50} = 750.0 \pm 10.0 \mu\text{M}$). This compound also was found to be the most active derivative among all of the synthesized compounds. On the other hand, compound 8o

showed two-fold higher activity compared to its counterpart 8f ($IC_{50} = 130.7 \pm 1.5 \mu M$) in Category A. Compound 8k ($IC_{50} = 77.0 \pm 0.5 \mu M$) with methyl substitution was identified as the second most potent derivative in this series and also among all synthesized compounds. This compound was also showed two-fold higher activity in comparison to its counterpart 8b in Category A. Therefore, as emphasized in the Category A, it seems that electronic properties have no significant effect on the inhibitory activity. The introduction of a hydroxyl and methoxy group as R_1 in compounds 8p ($IC_{50} = 86.3 \pm 0.6 \mu M$) and 8l ($IC_{50} = 89.6 \pm 0.7 \mu M$), respectively, led to a slight reduction in inhibitory activity. These compounds were the third most active analogs among all screened compounds and compared with their counterparts 8g and 8c in Category A, about 1.5-2 fold increased activity were observed. In the case of halogenated compounds in this series, the replacement of the hydroxyl or methoxy groups with an electron withdrawing chloro group in compound 8m ($IC_{50} = 115.7 \pm 1.3 \mu M$) reduced the inhibitory efficacy. On the other hand, 8n was more active than its counterpart 8e in category A. Switching from chloro to bromo group in compound 8n ($IC_{50} = 506.2 \pm 8.5 \mu M$) led to a dramatic decrease in the inhibitory activity which, in contrast to Category A, reduced its activity by more than four-fold comparison to chlorinated compound 8e. It is also interesting to note that the unsubstituted derivative 8j ($IC_{50} = 387.7 \pm 5.0 \mu M$) in series B demonstrated less inhibitory activity and its activity was four-fold lower than its counterpart in Category A (8a).

According to the comparison of IC_{50} values of derivatives in two groups, except analogs 8j and 8n (un-substituted and 4-bromo derivatives, respectively), all other derivatives in Category B were more active than their counterparts in the first category. Thus, based on the limited structure-activity relationship, it can be concluded that the presence of a methyl group in R_2 played a more effective role in *in vitro* α -glucosidase inhibitory activity compared with effect of the change of substituent in the R_1 position. It seems that the presence of the methyl group led to a better fit of the phenyl group in the pocket of α -glucosidase enzyme. *In silico* molecular modeling was also performed in order to obtain a better understanding of the effect of different structural motifs of these novel derivatives in their binding modes with the active site of α -glucosidase enzyme.

Please insert Table 1 about here

2.3. Inhibition kinetics of α -glucosidase

In order to gain further insight into the inhibition mechanism of the synthesized compounds on α -glucosidase, kinetic study was performed on the most potent compound 8o according to our previous report [63-66]. The mode of inhibition was determined by Lineweaver–Burk plots and then K_i was calculated with secondary re-plot of Lineweaver–Burk plots. The analysis of obtained Lineweaver–Burk plots showed that, with increasing concentrations of compound 8o, V_{max} value remained unchanged while the K_m increased. It indicated that compound 8o was a competitive inhibitor and competed with the substrate for binding to the active site of α -glucosidase (Fig. 3a). Moreover, secondary re-plot of mentioned Lineweaver–Burk plots against the different concentrations of compound 8o provided an estimate of the inhibition constant, K_i values of 87.0 μ M for compound 8o (Fig. 3b).

Similarly, recently, new bis-azo-containing Schiff base possessed nitro groups was synthesized which also competitively inhibited the α -glucosidase [67]. Interestingly, to the best of our knowledge, none of the reported pyrazole-based inhibitor competitively inhibited the enzyme activity.

Please insert Fig. 3 about here

2.4. Cytotoxic activity

In order to determine the toxicities of the most potent compounds (8o, 8k, 8p, 8l, 8i, and 8a), The MTT assay was conducted on normal 3T3 cell line. The results of cytotoxic activity were expressed as the IC_{50} (μ M) and outlined in Table 2. Results revealed that the selected compounds depicted no cytotoxic activity against 3T3 cells with IC_{50} value $> 50 \mu$ M, showing that these compounds have a high level of safety profile.

[Please insert Table 2 about here]

2.5. Computational methods

2.5.1. Homology modeling

Since the crystallographic structure of the protein has not been obtained yet, the homology modeling technique was used to generate three-dimensional (3D) structure of the protein. Molecular docking was performed by modeled 3D structure. The primary sequence of *Saccharomyces cerevisiae* α -glucosidase was retrieved from the Uniprot in FASTA format (Access code P53341) and searched in Protein BLAST against the PDB structures to get template [68]. As a result, the X-ray crystal structure of α -D-glucose bound isomaltase from *S. cerevisiae* (PDB ID: 3A4A) was chosen as a template for the homology modeling due to its highest sequence identity among the other templates [69]. Before the modeling process, alignment of the target and template sequences were performed using the multiple sequence alignment method. The selected template showed sequence identity and similarity of 71.4 % and 86.7 %, respectively (Fig. S1 in Supplementary). The 3D structural model of α -glucosidase for *S. cerevisiae* was obtained using the “Build Homology Models” module in Discovery Studio 4.1. A set of 10 intermediate models were generated. The best model was selected based on the lowest PDF Total Energy (3270.6404) and DOPE Scores (-73110.257813) and evaluated for further validation (see details in Supplementary Data).

2.5.2. Molecular docking study

Docking simulation was employed to identify the possible binding mode of the most active inhibitors in the active site of the developed homology model of α -glucosidase by employing the GOLD 5.3.0 tool. Before docking and analysis of the binding mode, docking method was validated by redocking the co-crystallized acarbose and α -D-glucopyranose in binding site of α -glucosidase from Sugar beet (PDB code: 3W37) and isomaltase from Baker's yeast (PDB code: 3A4A), respectively. The RMSD value between best docked and actual pose of acarbose and α -D-glucopyranose were found to be 1.12 Å and 0.96 Å, respectively, which indicated the reliability of the method (Fig. S2 in Supplementary).

Acarbose as standard drug and the synthesized compounds were docked in the active site of modeled α -glucosidase. The docking results revealed that all the synthetic compounds showed significant *in silico* inhibitory activities and exhibited prominent gold fitness docking scores ranging from 36.72 to 62.78 that showed the best accommodation of all the compounds in the active site of the enzyme. Investigation of ligand-protein interactions of synthetic derivatives

indicated that the compounds in which the substituent has either EWG or EDG showed good *in silico* inhibition. Analysis of the predicted binding conformations showed that diphenyl pyrazole moiety could be completely inserted into the hydrophobic site pocket through pi-pi or pi-cation interactions with residues of the enzyme. Besides, carbonyl oxygen atoms and NH of hydrazone linker form hydrogen bonds to improve the docking affinity with α -glucosidase. The detailed binding mode of acarbose revealed that this drug formed hydrogen bonding interactions with residues Asn241, Gln181, His348, Glu276, Asp68 and hydrophobic interaction with residues Ala278 and Phe157 (Fig. 4b). For more investigation, detailed binding modes of most potent compounds 8o, 8k, 8p, 8l, and 8i were also shown in Fig. 4c-f. Compound 8o is the most potent compound in all of the synthesized compounds and well fitted into the binding cavity of α -glucosidase (Fig. 4c). Several hydrophobic interactions were observed between 1, 3-diphenyl pyrazole moiety and the active site residues, viz., Arg429, Tyr71, Phe157, Phe177, and Ala278 which stabilizes the binding of compound 8o in the active site of the enzyme. Asp68 formed a strong hydrogen bond with oxygen of the nitro substituent. Whereas, residues Ala278 and His279 formed a pi-alkyl interaction with methyl substituent on the phenyl ring. This interaction seems to justify partial high potency of Category B compared to Category A. Asp408 formed H-acceptor interaction with nitrogen atom of hydrazone linker and an H-donor interactions were observed between Arg439 and Tyr313 and carbonyl oxygen atoms which further stabilized the enzyme-inhibitor complex. Moreover, Arg312 and Arg349 involved in aren-alkyl interaction with the phenyl ring of the semicarbazide moiety and a pi-hydrogen interaction was also found between Arg312 and pi system of the ring. Compound 8k, the second most active compound, showed considerable hydrogen bonding interactions with the active site residues. The binding mode of compound 8k is shown in Fig. 4d. Asp349 formed hydrogen acceptor interaction with the NH groups of semicarbazide moiety while Arg212 and Asp214 formed H-donor interactions with the oxygen atom of the carbonyl group. In addition, compound 8k also established some important hydrophobic interactions with Ala278, Phe157, Phe300, Arg 312, Arg 439, Tyr313, and Leu437. Furthermore, 4-methyl substituent in R₁ position established pi-alkyl interactions with Ala278, Phe157, and His245. The third and the fourth most potent compounds 8p (4-hydroxy on R₁ position) and 8l (4-methoxy on R₁ position) showed almost similar interaction with the active site, as shown in Fig. 4e. This observation confirmed by the obtained results of *in vitro* assay. Comparing the binding mode of compound 8p and 8l, it was revealed that the lone

pair of oxygen atom, in both hydroxyl and methoxy substitutions, interacted with Tyr71 while in compound 8l Asp68 formed an H-acceptor interaction with the CH₃ of methoxy substituent. Compound 8i is the fourth most active among all of the synthesized compounds and most active in Category A. Similar to other compounds, 1, 3-diphenyl pyrazole moiety is positioned in a hydrophobic pocket formed by Phe177, Phe157, Ala278, Glu276, Leu218, and Ala278 while CF₃ substituent interacted with residues As68, Arg439 and Tyr71. Gln350 formed an H-acceptor interaction with the NH of semicarbazide moiety and Arg312 displayed a hydrogen donor interaction with the carbonyl of the same moiety. Also, terminal phenyl group showed pi-alkyl interaction with Arg439 (Fig. 4f).

Comparing the binding mode of A and B categories indicated that both series showed interactions with almost similar active site residues. Based on docking results, more biological activity of Category B might be due to the interaction with more active site residues as compare to Category A. The slight difference in the binding modes of compounds in A and B series was in good agreement with those results obtained in *in vitro* assay. The molecular docking study showed that all synthesized compounds had a good binding affinity towards the binding site of α -glucosidase enzyme. The higher binding affinity for these compounds is presumably attributed to strong binding contributed by the higher number of stable hydrogen bonds and hydrophobic interactions between the reactive pharmacophore and amino acids in the active site of the enzyme. As previous studies have confirmed, hydrogen bonding and hydrophobic interactions may be the important factors affecting the enhancement of inhibitory activity [22].

The minimum energy of interaction between the ligand and active site of α -glucosidase enzyme was obtained as gold fitness as a scoring function. The calculated docking score of most potent compounds was significantly more than that of acarbose (35.71). The compounds 8o, 8k and 8l displayed best docking scores with values of 62.78, 61.24 and 58.59 which are highly correlated with *in vitro* α -glucosidase inhibition activity.

Please insert Fig. 4 about here

2.5.3. Molecular dynamic investigation

Additionally MD simulation was performed in order to understand the effect of the most active compound over the enzyme active site. For this purpose, the structural perturbations incurred by the most potent compound (compounds 8o) have been investigated through study the RMSD and RMSF and its effect on the active site environment in comparison to acarbose as α -glucosidase standard inhibitor.

Root mean square deviation (RMSD) of the enzymes's C α was analyzed over 20 ns MD simulation in order to study the stability of the protein-ligand complex. It showed that the RMSD of the apo α -glucosidase is lower than the two enzyme complexes and its values decreased after about 5 ns and became more stable at 1.5 Å with lower fluctuation towards the end of the simulation. This means that the RMSD of the bounded state enzymes deviate from the initial structure of apo enzyme in the early part of the simulation as a result of structural flexibility. It is expected that compound 8o had higher RMSD than acarbose for its higher number of rotatable bond and flexibility which makes it more deviate from the initial structure. α -glucosidase complexed with compound 8o and acarbose maintained an overall stability for the most part of simulation time with fluctuation stabilizing at an average of 2.63 Å and 2.1 Å, respectively (Fig. S3 in Supplementary). Such observation indicated that the employed simulation time was enough to obtain an equilibrium structure over the simulation time. Thus, the structures at the MD equilibrium state was used to investigate the structural specificity of the ligand-protein complexes.

The RMSF, which indicated the flexibility of the protein structure, was referred to the fluctuation of the C α atom from its average position throughout the simulation time. Comparing RMSF values of α -glucosidase-compound complexes show that the residues of the conserved region I (106-111), II (210-28), III (276-279), and IV (344-349) would have the same RMSF value in α -glucosidase-acarbose and α -glucosidase-8o complexes (Fig. 5). Based on the observed result of RMSF plot, although α -glucosidase-acarbose complex showed residues at the entrance region loop covering the active site (310-315) have lower RMSF value than in α -glucosidase-8o complex (green box), the other lid loop covering the active site consists of residues 230-236 [70] showed significantly lower RMSF value in α -glucosidase-8o complex (pink box) rather than α -glucosidase-acarbose complex.

Fig. 6a and 6b represent the detailed orientation and interactions that occurred more than 30% of the simulation time during the equilibrated phase over α -glucosidase complexed with compound 8o. The interaction analysis depicted that compound 8o oriented horizontally at the bottom of the active site and stabilized the enzyme domains by interacting with Tyr71, Arg443, Asp349 and Arg439 from domain A and Phe158 and Phe177 from domain B (Fig. 6a). On the other hand, acarbose oriented vertically and formed non-binding interaction with the Phe311, Asn241, Arg439, Asp68, His245, Asp349, and Asp214 which belong to the domain A of the enzyme (Fig. 6c). This observation may propose the contribution to the higher α -glucosidase inhibition activity.

Comparing the MD simulation of compound 8o and acarbose revealed a long lasting non-binding interaction with Asp439, Asp68 and Arg439 proposed to have a significant role on the inhibition activity of the mentioned compounds (Fig. 6c).

Fig. 6b represented compound 8o formed H bond interaction through the semicarbazone linker with the conserved catalytic residue Asp249 and Glu304 for about 96% of MD simulation time which is similar to the behavior of the NH₂ group in the acarbose. Moreover, the para nitro phenyl group oriented toward the interface of domain A and B through strong ionic interaction of the nitro group with Asp68 and Arg439, π -cation and π - π hydrophobic interaction with Phe177 and Arg443 at the wall of the active site, and Tyr71 at the bottom of the active site. It was obvious from the MD study that H-bonding and hydrophobic interactions had critical role in stabilizing compound 8o at the bottom of the active site during the simulation time and caused α -glucosidase inhibition activity.

In addition to the interaction analysis, the Prime/MM-GBSA module was used to estimate the strengths of interactions between the ligand-protein complexes which generated by the clustering method. ΔG_{bind} of α -glucosidase/compound 8o complex and α -glucosidase/acarbose complex were estimated to be -74.83 and -62.49 kcal/mol, respectively, revealing stronger binding interaction of compound 8o than acarbose which also supported by experimental assay.

Please insert Fig. 5 about here

Please insert Fig. 6 about here

2.6. Conclusion

In conclusion, a novel series of pyrazole-phenyl semicarbazone hybrids were designed and synthesized as potential α -glucosidase inhibitors. The docking results rationalized the idea of hybridization. As a result, designed hybrid packed in the catalytic hydrophobic pocket of the active site while nitrogen and oxygen atoms of the semicarbazide formed hydrogen bonds with the enzyme. It is worth mentioning that inhibitory activity of all new designed compounds in the range of 1-12 fold were better than acarbose. Among them, the most potent compound was 1-((3-(4-nitrophenyl)-1-p-tolyl-1H-pyrazol-4-yl)methylene)-4-phenylsemicarbazide 8o with IC_{50} value of 65.1 μ M is around 12-fold more active than acarbose as the standard drug. Also, analysis of the kinetic of enzyme inhibition indicated that this compound can inhibit α -glucosidase via a competitive mechanism. The analysis of the structure-activity relationship revealed that electronic properties of substitutions in R_1 did not have much effect on inhibitory potential. The cytotoxicity assays confirmed that most potent compounds (8o, 8k, 8p, 8l, 8i, and 8r) showed no cytotoxicity against 3T3 cell line. The docking study predicted that most potent compounds bind to the active site of the modeled α -glucosidase through the multiple hydrogen bonds and hydrophobic interactions. In addition, MD simulations showed compound 8o oriented horizontally at the bottom of the active site and stabilized the enzyme domains by interacting with the interface of domain A and domain B while acarbose oriented vertically and formed non-binding interactions with the residue belong to the domain A of the enzyme. Moreover, semicarbazone linker provided such a strategic point with the ability to interact with the Asp349 which has the catalytic role for α -glucosidase activity.

Based on these studies, it is assumed that the newly identified inhibitors may serve as lead molecules for further research for getting powerful α -glucosidase inhibitors.

3. Experimental

All reagents and solvents used in this study were purchased from Sigma Aldrich (USA) and Merck (Germany) and were used without further purification. All the reactions were monitored on pre-coated silica gel aluminum plates (Merck silica gel 60, F254) and visualized using UV lamp at 254 nm (UVGL-58; Upland, USA). Melting points of the target compounds 8a-p were

determined with a Kofler hot stage apparatus and are uncorrected. The IR spectra recorded with Nicolet FT-IR Magna 550 spectrographs using KBr pellets from 400 to 4000 cm^{-1} . ^1H and ^{13}C NMR spectra were recorded on a Bruker FT-500 in DMSO- d_6 using TMS as internal standard. Elemental analysis was carried out on Elementar Analysen system GmbH VarioEL CHNS mode.

3.1. General procedure for the synthesis of pyrazole-4-carbaldehydes **4a-p**

Different substituted acetophenone **1** (10 mmol), phenyl hydrazine or 4-methyl phenyl hydrazine **2** (12 mmol) and 1 ml of sulfuric acid as catalyst was being dissolved in 15 mL of ethanol and refluxed for 8-12 h. Once the completion of the reaction was confirmed by TLC, the reaction mixture was poured into ice bath to complete the crystallization. The precipitated hydrazone intermediate **3a-p** were filtered off, washed with water, and purified by recrystallization in ethanol. In the next step, resulted hydrazone derivative (10 mmol) (**3a-p**) was added to a solution of DMF (6 mL) and POCl_3 (30 mmol) and the reaction was heated at 60 $^\circ\text{C}$ for 5-8 h. The reaction was monitored by TLC. After completing the reaction, the mixture was cooled to room temperature and added 20 mL of ice-cold water. After neutralizing the mixture with a saturated solution of sodium hydroxide, the solid product was filtered, washed with water, dried and recrystallized from ethanol [22].

3.2. General procedure for the synthesis of phenyl urea **6**

50 mmol of sodium cyanate in 80 ml of warm water was added to a stirring solution of aniline **5** (50 mmol) in 20 ml of glacial acetic acid and 10 ml of water. The reaction mixture was allowed to stand for 30 min at 0-5 $^\circ\text{C}$ in ice-water bath. Then, the obtained precipitate was filtered and recrystallized from boiling water to obtain pure phenyl urea **6** [60, 71].

3.3. General procedure for the synthesis of phenyl semicarbazide **7**

A mixture of 50 mmol phenyl urea **6** and equimolar quantities of hydrazine hydrate (2.5 mL) in ethanol (50 mL) was refluxed for 12 h in the presence of 50 mmol sodium hydroxide. After completion of reaction (checked by TLC), the two-third volume of ethanol were evaporated and

then poured into ice. The resultant precipitate was filtered, dried, and then crystallized from ethanol and yielded phenyl semicarbazide 7 [60, 71].

3.4. General procedure for the synthesis pyrazole-phenyl semicarbazone hybrids **8a-p**

The final step involves the condensation of various pyrazole carbaldehydes with phenyl semicarbazide. A solution of substituted pyrazole-4-carbaldehydes 4a-p (0.5 mmol), phenyl semicarbazide 7 (0.6 mmol) in 15 mL of ethanol was heated at reflux in the presence of a catalytic amount of glacial acetic acid for 8-12 h. Progress monitored using TLC and after completion of the reaction, two-third volume of solvent was being removed using rotary evaporator. The mixture was cooled down to room temperature. The resulting precipitate was filtered off, washed with ethanol, and purified by recrystallization in ethanol.

3.4.1. 1-((1,3-diphenyl-1H-pyrazol-4-yl)methylene)-4-phenylsemicarbazide (8a)

Pale yellow crystals; yield: 83%, mp 213-215 °C. IR (KBr, cm^{-1}): 3390 (N-H), 3141, 2883 (Ar-H), 1683 (C=O), 1610 (C=N), 1577, 1454 (C=C). ^1H NMR (400 MHz, $\text{DMSO-}d_6$) δ 10.65 (s, 1H, CO-NH), 9.21 (s, 1H, N-NH), 8.55 (s, 1H, H_5 -pyr), 8.08 (s, 1H, -CH=), 7.98 – 7.93 (m, 2H, Ar-H), 7.73 – 7.68 (m, 2H, Ar-H), 7.64 – 7.46 (m, 8H, Ar-H), 7.43 – 7.37 (m, 1H, Ar-H), 7.35 – 7.28 (m, 2H, Ar-H), 7.06 – 7.00 (m, 1H, Ar-H). Anal. Calcd for $\text{C}_{23}\text{H}_{19}\text{N}_5\text{O}$: C, 72.42; H, 5.02; N, 18.36; O, 4.19. Found: C, 72.36; H, 4.83; N, 19.10.

3.4.2. 4-phenyl-1-((1-phenyl-3-p-tolyl-1H-pyrazol-4-yl)methylene)semicarbazide (8b)

Pale yellow crystals; yield: 78%, mp 212-214 °C. IR (KBr, cm^{-1}): 3378 (N-H), 3067, 2933 (Ar-H), 1683 (C=O), 1597 (C=N), 1526, 1439 (C=C). ^1H NMR (400 MHz, $\text{DMSO-}d_6$) δ 10.80 (s, 1H, CO-NH), 9.32 (s, 1H, N-NH), 8.75 (s, 1H, H_5 -pyr), 8.20 (s, 1H, -CH=), 8.09 – 8.05 (m, 2H, Ar-H), 7.75 – 7.68 (m, 6H, Ar-H), 7.55 – 7.41 (m, 5H, Ar-H), 7.19 – 7.13 (m, 1H, Ar-H), 2.53 (s, 3H, CH_3). ^{13}C NMR (101 MHz, DMSO) δ 152.71 (C=O), 151.02 (C3-pyr), 139.06, 138.87(-CH=), 137.95, 133.38, 129.65, 129.47, 129.26, 128.54, 128.14, 127.65, 126.83 (C5-pyr), 122.44, 119.40, 118.51, 117.08 (C4-pyr), 20.85 (CH_3). Anal. Calcd for $\text{C}_{24}\text{H}_{21}\text{N}_5\text{O}$: C, 72.89; H, 5.35; N, 17.71; O, 4.05. Found: C, 73.13; H, 4.96; N, 17.35.

3.4.3. 1-((3-(4-methoxyphenyl)-1-phenyl-1H-pyrazol-4-yl)methylene)-4-phenylsemicarbazide (8c)

Pale yellow crystals; yield: 75%, mp 288-290 °C. IR (KBr, cm^{-1}): 3397 (N-H), 3110, 2920 (Ar-H), 1694 (C=O), 1616 (C=N), 1599, 1523 (C=C), 1250 (C-OCH₃). ¹H NMR (400 MHz, DMSO-*d*₆) δ 10.79 (s, 1H, CO-NH), 9.31 (s, 1H, N-NH), 8.76 (s, 1H, H₅-pyr), 8.20 (s, 1H, -CH=), 8.09 – 8.05 (m, 2H, Ar-H), 7.79 – 7.67 (m, 6H, Ar-H), 7.55 – 7.49 (m, 1H, Ar-H), 7.48 – 7.42 (m, 2H, Ar-H), 7.25 – 7.20 (m, 2H, Ar-H), 7.20 – 7.13 (m, 1H, Ar-H), 3.96 (s, 3H, OCH₃). ¹³C NMR (101 MHz, DMSO) δ 159.47 (C-O), 152.72 (C=O), 150.88 (C3-pyr), 139.07, 138.89 (-CH=), 133.47, 129.64, 129.56, 128.53, 127.56, 126.76 (C5-pyr), 124.65, 122.44, 119.41, 118.45, 116.92 (C4-pyr), 114.11, 55.21 (CH₃O-). Anal. Calcd for C₂₄H₂₁N₅O₂: C, 70.06; H, 5.14; N, 17.02; O, 7.78. Found: C, 70.55; H, 5.73; N, 16.76.

3.4.4. 1-((3-(4-chlorophenyl)-1-phenyl-1H-pyrazol-4-yl)methylene)-4-phenylsemicarbazide (8d)

Pale yellow crystals; yield: 84%, mp 287-289 °C. IR (KBr, cm^{-1}): 3230 (N-H), 3123, 3050 (Ar-H), 1670 (C=O), 1593 (C=N), 1561, 1420 (C=C), 1012 (C-Cl). ¹H NMR (400 MHz, DMSO-*d*₆) δ 10.86 (s, 1H, CO-NH), 9.38 (s, 1H, N-NH), 8.77 (s, 1H, H₅-pyr), 8.22 (s, 1H, -CH=), 8.12 – 8.06 (m, 2H, Ar-H), 7.90 – 7.85 (m, 2H, Ar-H), 7.77 – 7.68 (m, 6H, Ar-H), 7.56 – 7.50 (m, 1H, Ar-H), 7.48 – 7.41 (m, 2H, Ar-H), 7.13 – 7.13 (m, 1H, Ar-H). ¹³C NMR (101 MHz, DMSO) δ 152.67 (C=O), 149.68 (C3-pyr), 138.95, 138.89 (-CH=), 133.29, 133.04, 131.20, 129.99, 129.67, 128.75, 128.55, 128.09, 127.01 (C5-pyr), 122.42, 119.36, 118.59, 117.27 (C4-pyr). Anal. Calcd for C₂₃H₁₈ClN₅O: C, 66.43; H, 3.36; Cl, 8.52; N, 16.84; O, 3.85. Found: C, 66.79; H, 3.86; N, 15.21.

3.4.5. 1-((3-(4-bromophenyl)-1-phenyl-1H-pyrazol-4-yl)methylene)-4-phenylsemicarbazide (8e)

Pale yellow crystals; yield: 86%, mp > 300 °C. IR (KBr, cm^{-1}): 3301 (N-H), 3139, 2920 (Ar-H), 1617 (C=O), 1593 (C=N), 1552, 1490 (C=C). ¹H NMR (400 MHz, DMSO-*d*₆) δ 10.82 (s, 1H, CO-NH), 9.34 (s, 1H, N-NH), 8.71 (s, 1H, H₅-pyr), 8.19 (s, 1H, -CH=), 8.12 – 8.03 (m, 2H, Ar-H), 7.92 – 7.78 (m, 4H, Ar-H), 7.72 (m, 4H, Ar-H), 7.57 – 7.41 (m, 3H, Ar-H), 7.21 – 7.13 (m, 1H, Ar-H). ¹³C NMR (101 MHz, DMSO) δ 152.65 (C=O), 149.74 (C3-pyr), 138.94, 138.83 (-CH=), 133.01, 131.66, 131.57, 130.28, 129.69, 128.58, 128.13, 127.04 (C5-pyr), 122.46,

121.97, 119.35, 118.60, 117.23 (C4-pyr). Anal. Calcd for $C_{23}H_{18}BrN_5O$: C, 60.01; H, 3.94; Br, 17.36; N, 15.21; O, 3.48. Found: C, 60.55; H, 3.42; N, 14.82.

3.4.6. 1-((3-(4-nitrophenyl)-1-phenyl-1H-pyrazol-4-yl)methylene)-4-phenylsemicarbazide (8f)

Pale yellow crystals; yield: 82%, mp > 300 °C. IR (KBr, cm^{-1}): 3375 (N-H), 3138, 2960 (Ar-H), 1677 (C=O), 1605 (C=N), 1598, 1446 (C=C), 1534, 1350 (C-NO₂). ¹H NMR (400 MHz, DMSO-*d*₆) δ 10.87 (s, 1H, CO-NH), 9.40 (s, 1H, N-NH), 8.75 (s, 1H, H₅-pyr), 8.55 – 8.47 (m, 2H, Ar-H), 8.25 (s, 1H, -CH=), 8.20 – 8.14 (m, 2H, Ar-H), 8.14 – 8.07 (m, 2H, Ar-H), 7.78 – 7.67 (m, 4H, Ar-H), 7.56 (t, *J* = 7.4 Hz, 1H), 7.44 (t, *J* = 7.9 Hz, 2H), 7.20 – 7.13 (m, 1H, Ar-H). ¹³C NMR (101 MHz, DMSO) δ 152.65 (C=O), 148.59 (C-NO₂), 147.12 (C3-pyr), 138.82, 138.80 (-CH=), 132.65, 129.73, 129.25, 128.58, 128.54, 127.35 (C5-pyr), 123.91, 122.51, 119.41, 118.78, 117.92 (C4-pyr). Anal. Calcd for $C_{23}H_{16}N_6O_3$: C, 64.78; H, 4.25; N, 19.71; O, 11.26. Found: C, 64.22; H, 4.52; N, 20.12.

3.4.7. 1-((3-(4-hydroxyphenyl)-1-phenyl-1H-pyrazol-4-yl)methylene)-4-phenylsemicarbazide (8g)

Pale yellow crystals; yield: 86%, mp 204–206 °C. IR (KBr, cm^{-1}): 3360 (N-H), 1688 (C=O), 1599 (C=N), 1536, 1442 (C=C). ¹H NMR (400 MHz, DMSO-*d*₆) δ 10.75 (s, 1H, CO-NH), 9.90 (s, 1H, OH), 9.28 (s, 1H, N-NH), 8.73 (s, 1H, H₅-pyr), 8.19 (s, 1H, -CH=), 8.06 (d, *J* = 8.0 Hz, 2H, Ar-H), 7.80 – 7.59 (m, 6H, Ar-H), 7.48 (dt, *J* = 7.6, 25.3 Hz, 3H, Ar-H), 7.16 (t, *J* = 7.3 Hz, 1H, Ar-H), 7.05 (d, *J* = 8.2 Hz, 2H, Ar-H). ¹³C NMR (101 MHz, DMSO) δ 157.84 (C-OH), 152.75 (C=O), 151.31 (C3-pyr), 139.10, 138.93 (-CH=), 133.67, 129.62, 129.55, 128.54, 127.34, 126.68 (C5-pyr), 122.26, 122.41, 119.43, 118.39, 116.78 (C4-pyr), 115.46. Anal. Calcd for $C_{23}H_{19}N_5O_2$: C, 69.51; H, 4.82; N, 17.62; O, 8.05. Found: C, 69.85; H, 4.24; N, 16.80.

3.4.8. 1-((3-(4-fluorophenyl)-1-phenyl-1H-pyrazol-4-yl)methylene)-4-phenylsemicarbazide (8h)

Pale yellow crystals; yield: 90%, mp 228–230 °C. IR (KBr, cm^{-1}): 3129 (N-H), 3015, 2913 (Ar-H), 1697 (C=O), 1613 (C=N), 1530, 1499 (C=C), 1243 (C-F). ¹H NMR (400 MHz, DMSO-*d*₆) δ 10.80 (s, 1H, CO-NH), 9.34 (s, 1H, N-NH), 8.77 (s, 1H, H₅-pyr), 8.19 (s, 1H, -CH=), 8.08 (d, *J* = 8.0 Hz, 2H, Ar-H), 7.89 (dd, *J* = 5.5, 8.4 Hz, 2H, Ar-H), 7.78 – 7.48 (m, 7H, Ar-H), 7.45 (t, *J* = 7.7 Hz, 2H, Ar-H), 7.17 (t, *J* = 7.4 Hz, 1H, Ar-H). ¹³C NMR (101 MHz, DMSO) δ 162.26 (d, *J* = 246.4 Hz, C-F), 152.69 (C=O), 150.06 (C3-pyr), 138.99, 138.86 (-CH=), 133.13, 130.41,

130.32, 129.67, 128.77, 128.74, 128.54, 127.72, 126.97 (C5-pyr), 122.47, 119.44, 118.56, 117.15 (C4-pyr), 115.79, 115.57. Anal. Calcd for C₂₃H₁₈FN₅O: C, 69.16; H, 4.54; F, 4.76; N, 17.53; O, 4.01. Found: C, 64.18; H, 4.93; N, 16.95.

3.4.9. 4-phenyl-1-((1-phenyl-3-(4-(trifluoromethyl)phenyl)-1H-pyrazol-4-yl)methylene)semicarbazide (8i)

Pale yellow crystals; yield: 92%, mp 258-260 °C. IR (KBr, cm⁻¹): 3233 (N-H), 3018, 2950 (Ar-H), 1699 (C=O), 1605 (C=N), 1500, 1496 (C=C), 1303 (C-F). ¹H NMR (400 MHz, DMSO-*d*₆) δ 10.82 (s, 1H, CO-NH), 9.38 (s, 1H, N-NH), 8.72 (s, 1H, H₅-pyr), 8.23 (s, 1H, -CH=), 8.13 – 8.01 (m, 6H, Ar-H), 7.77 – 7.68 (m, 4H, Ar-H), 7.56 (td, *J* = 1.2, 7.3 Hz, 1H, Ar-H), 7.47 – 7.40 (m, 2H, Ar-H), 7.20 – 7.13 (m, 1H, Ar-H). ¹³C NMR (101 MHz, DMSO) δ 152.64 (C=O), 149.36 (C3-pyr), 138.90, 138.80 (-CH=), 136.41, 132.85, 129.72, 129.37, 128.98, 128.84, 128.53, 128.34, 127.19 (C5-pyr), 125.63, 125.59, 125.55, 122.49, 119.35, 118.69, 117.56 (C4-pyr). Anal. Calcd for C₂₄H₁₈F₃N₅O: C, 64.14; H, 4.34; F, 12.68; N, 15.58; O, 3.56. Found: C, 63.70; H, 4.52; N, 16.09.

3.4.10. 4-phenyl-1-((3-phenyl-1-p-tolyl-1H-pyrazol-4-yl)methylene)semicarbazide (8j)

Pale yellow crystals; yield: 81%, mp 223-225 °C. IR (KBr, cm⁻¹): 3325 (N-H), 3073, 2923 (Ar-H), 1702 (C=O), 1574 (C=N), 1501, 1480 (C=C). ¹H NMR (400 MHz, DMSO-*d*₆) δ 10.78 (s, 1H, CO-NH), 9.30 (s, 1H, N-NH), 8.80 (s, 1H, H₅-pyr), 8.21 (s, 1H, -CH=), 8.00 – 7.94 (m, 2H, Ar-H), 7.85 – 7.80 (m, 2H, Ar-H), 7.79 – 7.73 (m, 2H, Ar-H), 7.71 – 7.58 (m, 3H, Ar-H), 7.54 – 7.42 (m, 4H, Ar-H), 7.17 (tt, *J* = 1.2, 7.3 Hz, 1H, Ar-H), 2.51 (s, 3H, CH₃). ¹³C NMR (101 MHz, DMSO) δ 152.74 (C=O), 150.79 (C3-pyr), 138.90 (-CH=), 136.85, 136.31, 133.38, 132.30, 130.02, 128.71, 128.53, 128.45, 128.21, 127.35 (C5-pyr), 122.45, 119.50, 118.44, 116.97 (C4-pyr), 20.48 (CH₃). Anal. Calcd for C₂₄H₂₁N₅O: C, 72.89; H, 5.35; N, 17.71; O, 4.05. Found: C, 73.41; H, 5.82; N, 17.33.

3.4.11. 1-((1,3-dip-tolyl-1H-pyrazol-4-yl)methylene)-4-phenylsemicarbazide (8k)

Pale yellow crystals; yield: 85%, mp 276-279 °C. IR (KBr, cm⁻¹): 3365 (N-H), 3139, 2924 (Ar-H), 1685 (C=O), 1596 (C=N), 1578, 1420 (C=C). ¹H NMR (400 MHz, DMSO-*d*₆) δ 10.78 (s, 1H, CO-NH), 9.27 (s, 1H, N-NH), 8.75 (s, 1H, H₅-pyr), 8.20 (s, 1H, -CH=), 7.98 – 7.92 (m,

2H, Ar-H), 7.72 (dd, $J = 7.2, 8.4$ Hz, 4H, Ar-H), 7.54 – 7.41 (m, 6H, Ar-H), 7.20 – 7.12 (m, 1H, Ar-H), 2.52 (s, 3H, CH₃), 2.50 (s, 3H, CH₃). ¹³C NMR (101 MHz, DMSO) δ 152.73 (C=O), 150.78 (C3-pyr), 138.89 (-CH=), 137.87, 136.86, 136.21, 133.46, 130.00, 129.52, 129.24, 128.54, 128.12, 127.39 (C5-pyr), 122.43, 119.41, 118.38, 116.84 (C4-pyr), 20.85 (CH₃), 20.48 (CH₃). Anal. Calcd for C₂₅H₂₃N₅O: C, 73.33; H, 5.66; N, 17.10; O, 3.91. Found: C, 73.83; H, 5.15; N, 16.80.

3.4.12. 1-((3-(4-methoxyphenyl)-1-p-tolyl-1H-pyrazol-4-yl)methylene)-4-phenylsemicarbazide (8l)

Pale yellow crystals; yield: 80%, mp 224-226 °C. IR (KBr, cm⁻¹): 3372 (N-H), 3125, 2910 (Ar-H), 1670 (C=O), 1590 (C=N), 1580, 1468 (C=C), 1244 (C-OCH₃). ¹H NMR (400 MHz, DMSO-*d*₆) δ 10.77 (s, 1H, CO-NH), 9.25 (s, 1H, N-NH), 8.76 (s, 1H, H₅-pyr), 8.19 (s, 1H, -CH=), 7.98 – 7.93 (m, 2H, Ar-H), 7.79 – 7.72 (m, 4H, Ar-H), 7.53 – 7.41 (m, 4H, Ar-H), 7.25 – 7.20 (m, 2H, Ar-H), 7.19 – 7.13 (m, 1H, Ar-H), 3.96 (s, 3H, OCH₃), 2.50 (s, 3H, CH₃). ¹³C NMR (101 MHz, DMSO) δ 159.44 (C-O), 152.74 (C=O), 150.65 (C3-pyr), 138.91 (-CH=), 136.90, 136.13, 133.59, 129.98, 129.54, 128.52, 127.23 (C5-pyr), 124.75, 122.43, 119.42, 118.36, 116.68 (C4-pyr), 114.09, 55.21 (OCH₃), 20.47 (CH₃). Anal. Calcd for C₂₅H₂₃N₅O₂: C, 70.57; H, 5.45; N, 16.46; O, 7.52. Found: C, 70.97; H, 5.88; N, 15.92.

3.4.13. 1-((3-(4-chlorophenyl)-1-p-tolyl-1H-pyrazol-4-yl)methylene)-4-phenylsemicarbazide (8m)

Pale yellow crystals; yield: 91%, mp 287-289 °C. IR (KBr, cm⁻¹): 3349 (N-H), 3014, 2919 (Ar-H), 1694 (C=O), 1613 (C=N), 1580, 1452 (C=C), 1092 (C-Cl). ¹H NMR (400 MHz, DMSO-*d*₆) δ 10.79 (s, 1H, CO-NH), 9.29 (s, 1H, N-NH), 8.72 (s, 1H, H₅-pyr), 8.19 (s, 1H, -CH=), 7.99 – 7.94 (m, 2H, Ar-H), 7.93 – 7.84 (m, 2H, Ar-H), 7.77 – 7.70 (m, 4H, Ar-H), 7.54 – 7.41 (m, 4H, Ar-H), 7.16 (t, $J = 7.3$ Hz, 1H, Ar-H), 2.51 (s, 3H, CH₃). ¹³C NMR (101 MHz, DMSO) δ 152.67 (C=O), 149.46 (C3-pyr), 138.84 (-CH=), 136.75, 136.45, 133.23, 133.09, 131.25, 130.04, 129.97, 128.74, 128.56, 127.78 (C5-pyr), 122.46, 119.39, 118.48, 117.03 (C4-pyr), 20.49 (CH₃). Anal. Calcd for C₂₄H₂₀ClN₅O: C, 67.05; H, 4.69; Cl, 8.25; N, 16.29; O, 3.72. Found: C, 66.71; H, 4.15; N, 16.67.

3.4.14. 1-((3-(4-bromophenyl)-1-p-tolyl-1H-pyrazol-4-yl)methylene)-4-phenylsemicarbazide (8n)

Pale yellow crystals; yield: 89%, mp > 300 °C. IR (KBr, cm^{-1}): 3435 (N-H), 3156, 2915 (Ar-H), 1700 (C=O), 1610 (C=N), 1560, 1439 (C=C). ^1H NMR (400 MHz, $\text{DMSO-}d_6$) δ 10.76 (s, 1H, CO-NH), 9.26 (s, 1H, N-NH), 8.68 (s, 1H, H_5 -pyr), 8.19 (s, 1H, -CH=), 7.99 – 7.93 (m, 2H, Ar-H), 7.90 – 7.83 (m, 2H, Ar-H), 7.84 – 7.78 (m, 2H, Ar-H), 7.75 – 7.69 (m, 2H, Ar-H), 7.54 – 7.41 (m, 4H, Ar-H), 7.20 – 7.13 (m, 1H, Ar-H), 2.51 (s, 3H, CH_3). ^{13}C NMR (101 MHz, DMSO) δ 152.66 (C=O), 149.49 (C3-pyr), 138.84 (-CH=), 136.74, 136.45, 133.08, 131.64, 130.25, 130.03, 128.57, 127.86 (C5-pyr), 122.45, 121.89, 119.37, 118.48, 117.01 (C4-pyr), 20.49 (CH_3). Anal. Calcd for $\text{C}_{24}\text{H}_{20}\text{BrN}_5\text{O}$: C, 60.77; H, 4.25; Br, 16.84; N, 14.76; O, 3.37. Found: C, 59.95; H, 4.62; N, 14.33.

3.4.15. 1-((3-(4-nitrophenyl)-1-p-tolyl-1H-pyrazol-4-yl)methylene)-4-phenylsemicarbazide (8o)

Pale yellow crystals; yield: 84%, mp > 300 °C. IR (KBr, cm^{-1}): 3392 (N-H), 3079, 2938 (Ar-H), 1682 (C=O), 1598 (C=N), 1518, 1444 (C=C), 1372, 1332 (C-NO₂). ^1H NMR (400 MHz, $\text{DMSO-}d_6$) δ 10.86 (s, 1H, CO-NH), 9.36 (s, 1H, N-NH), 8.77 (s, 1H, H_5 -pyr), 8.53 – 8.47 (m, 2H, Ar-H), 8.28 (s, 1H, -CH=), 8.19 – 8.13 (m, 2H, Ar-H), 8.02 – 7.97 (m, 2H, Ar-H), 7.76 – 7.69 (m, 2H, Ar-H), 7.55 – 7.49 (m, 2H, Ar-H), 7.47 – 7.38 (m, 2H, Ar-H), 7.16 (t, $J = 7.2$ Hz, 1H, Ar-H), 2.51 (s, 3H, CH_3). ^{13}C NMR (101 MHz, DMSO) δ 152.65 (C=O), 148.29 (C3-pyr), 147.03 (C-NO₂), 138.87 (-CH=), 136.77, 136.63, 132.74, 130.07, 129.19, 128.52, 128.37 (C5-pyr), 123.88, 122.46, 119.41, 118.63, 117.74 (C4-pyr), 20.50 (CH_3). Anal. Calcd for $\text{C}_{24}\text{H}_{20}\text{N}_6\text{O}_3$: C, 65.45; H, 4.53; N, 19.08; O, 10.90. Found: C, 64.93; H, 4.85; N, 18.65.

3.4.16. 1-((3-(4-hydroxyphenyl)-1-p-tolyl-1H-pyrazol-4-yl)methylene)-4-phenylsemicarbazide (8p)

Pale yellow crystals; yield: 80%, mp 208-210°C. IR (KBr, cm^{-1}): 3320 (N-H), 1672 (C=O), 1580 (C=N), 1526, 1430 (C=C). ^1H NMR (400 MHz, $\text{DMSO-}d_6$) δ 10.75 (s, 1H, CO-NH), 9.96 (s, 1H, OH), 9.25 (s, 1H, N-NH), 8.81 (s, 1H, H_5 -pyr), 8.20 (s, 1H, -CH=), 7.95 (d, $J = 8.1$ Hz, 2H, Ar-H), 7.77 (d, $J = 8.0$ Hz, 2H, Ar-H), 7.64 (d, $J = 8.3$ Hz, 2H, Ar-H), 7.53 – 7.40 (m, 4H, Ar-H), 7.16 (t, $J = 7.3$ Hz, 1H, Ar-H), 7.06 (d, $J = 8.4$ Hz, 2H, Ar-H), 2.50 (s, 3H, CH_3). ^{13}C NMR (101 MHz, DMSO) δ 157.85 (C-OH), 152.76 (C=O), 151.08 (C3-pyr), 138.98 (-CH=),

136.92, 136.01, 133.79, 129.97, 129.49, 128.52, 127.11 (C5-pyr), 122.97, 122.37, 119.43, 118.27, 116.53 (C4-pyr), 115.47, 20.47 (CH₃). Anal. Calcd for C₂₄H₂₁N₅O₂: C, 70.06; H, 5.14; N, 17.02; O, 7.78. Found: C, 70.42; H, 5.61; N, 16.79.

3.5. *In vitro* α -glucosidase inhibition assay

The *in vitro* α -glucosidase inhibitory activities of pyrazole-phenyl semicarbazone hybrids 8a-p were carried out according to the protocol previously reported [72]. α -Glucosidase enzyme ((EC3.2.1.20, *Saccharomyces cerevisiae*, 20 U/mg) and substrate (p-nitrophenyl glucopyranoside) were purchased from Sigma Chemical Co. (St. Louis, MO, USA). Enzyme (50 mM) and the desired concentrations of nitrophenol- α -D-glucopyranoside (PNP) were prepared in potassium phosphate buffer (pH= 6.8). The stock solutions (10 mM) of standard and all tested compounds were dissolved in DMSO and further diluted with potassium phosphate buffer to prepare sample solutions in various concentrations. Firstly, the various concentrations of compounds 8a-p (20 μ L), enzyme solution (20 μ L) and potassium phosphate buffer (135 μ L) was pre-incubated at 37 °C for 10 min in a 96-well plate. After that, 25 μ L of substrate (p-nitrophenyl- α -Dglucopyranoside, 4 mM) was added to each well and then incubated at 37 °C for 20 min. The reaction was monitored spectrophotometrically by measuring the change in absorbance at 405 nm. DMSO and acarbose were used as the control and standard inhibitor, respectively. The percentage of enzyme inhibition for each entry was calculated by using the following formula:

$$\% \text{ Inhibition} = \frac{(\text{Abs control} - \text{Abs sample})}{\text{Abs control}} \times 100$$

IC₅₀ values of tested compounds were obtained from the nonlinear regression curve (logit method). All the tests were performed in triplicate and the results are expressed as the mean \pm SD

3.6. Kinetic studies

The mechanism of inhibition of the most potent compound 8o was investigated with different concentrations of p-nitrophenyl α -D-glucopyranoside as substrate in the absence and presence of compound 8o at different concentrations. The α -glucosidase solution (1 U/mL, 20 μ L) was incubated with different concentrations (0, 30, 45, and 65 μ M) of compound 8o (20 μ L) for the period of 15 min at 30 °C. Then, change in absorbance was measured for 20 min at 405 nm using spectrophotometer (Gen5, Power wave xs2, BioTek, America) following the adding different concentrations of p-nitrophenyl glucopyranoside (2–10 mM) as substrate. The inhibition types and the Michaelis–Menten constant (K_m) value were determined by Lineweaver-Burk plots. The experimental inhibitor constant (K_i) value was constructed by secondary plots of the inhibitor concentration [I] versus K_m .

3.7. Cytotoxicity evaluation of the most potent compounds on 3T3 cell line

The 3T3 cells were suspended in Dulbecco's modified Eagle medium (DMEM) formulated with 10% fetal bovine serum (FBS), 100 IU/mL streptomycin, and 100 IU/mL penicillin. The cells were plated at a concentration of 2×10^5 cells/mL and incubated overnight at 37 °C under 5% CO₂. Then supernatant was removed and 200 μ L fresh medium along with different concentrations of the selected compounds 8o, 8k, 8p, 8l, 8i, and 8a (0.04 to 50 μ M) were added and then further incubated for 48 h at 37 °C in CO₂ incubator. After treatment, the medium was aspirated carefully, and 50 μ L of MTT solution (2 mg/mL in PBS) was added to all wells. After 4 h of incubation, MTT solution was aspirated and 100 μ L DMSO was added to each well in order to dissolve the blue insoluble MTT formazan produced by the action of mitochondrial. Finally, the absorbance was recorded at 570 nm with a multi-well plate reader (Rayto, China) after agitating at room temperature for 10 min and readings were processed using MS Excel software. All the experiments were performed in triplicate.

3.8. Homology modeling

The amino acid sequence of *Saccharomyces cerevisiae* α -glucosidase was retrieved from UniProtKB database (UniProtKB, <http://www.uniprot.org/>) with accession number P53341. Hence, the sequence similarity search was performed using NCBI BLAST server (<https://blast.ncbi.nlm.nih.gov/Blast.cgi>) based on sequence identity. The crystal structures of isomaltase from *Saccharomyces cerevisiae* (PDB ID: 3A4A) selected as suitable template and retrieved from the Protein Data Bank. A sequence alignment between query and template was performed by Align sequence to template protocol in Discovery Studio (Accelrys, San Diego, CA) (DS). Finally, Homology modeling was performed with MODELER inbuilt in DS package. The number of models was set to 10 and the optimization level was set to “high”, whereas default values were set for other parameters.

DOPE score and profile-3D for preliminary evaluation of developed model were carried out using verify protein protocol in DS. Ramachandran plot and Verify3D with PROCHECK program (<http://servicesn.mbi.ucla.edu/PROCHECK>) were also applied to estimate the quality of the established model [73, 74]. Eventually, ProSA server was used for evaluation of the consistency between the modeled structure and the selected template [75].

3.9. Docking simulation

Molecular docking approach was performed using genetic algorithm based docking program (GOLD), which has been incorporated into Discovery Studio (DS) 4.1 to dock synthetic compounds against the α -glucosidase enzyme. 3D structure of internal ligands (acarbose and α -D-glucopyranose) and final synthesized derivatives were drawn using Chem Draw Ultra 12.0 software and were transferred into DS. Compounds were typed with CHARMM force field and partial charges were calculated by Momany-Rone option. Subsequently, resulting structures were minimized with Smart Minimizer algorithm which contains 1000 steps of steepest descent with a RMS gradient tolerance of 3, followed by Conjugate Gradient minimization. Later, 3D modeled structure of the α -glucosidase was subjected to protein preparation and minimization. The complex was typed with CHARMM force field, hydrogen atoms were added and pH of the protein was adjusted to almost neutral, 7.4, using protein preparation protocol in DS. A 9 Å radius sphere was defined as the binding region for docking study. Other parameters were set by default protocol settings [76]. All synthesized derivatives were docked into the active site of the

α -glucosidase and generated binding modes for each compound ranked by GOLD score fitness function.

3.10. Molecular dynamic simulation

Molecular dynamic (MD) simulation of this study was performed by using the Desmond v5.3 module implemented in Maestro interface (from Schrödinger 2018-4 suite) [77]. The appropriate pose for MD simulation procedure of the compounds was achieved by docking method.

In order to build the system for MD simulation, the protein-ligand complexes were solvated with SPC explicit water molecules and placed in the center of an orthorhombic box of appropriate size in the Periodic Boundary Condition. Sufficient counter-ions and a 0.15 M solution of NaCl were also utilized to neutralize the system and to simulate the real cellular ionic concentrations, respectively. The MD protocol involved minimization, pre-production, and finally production MD simulation steps. In the minimization procedure, the entire system was allowed to relax for 2500 steps by the steepest descent approach. Then the temperature of the system was raised from 0 to 300 K with a small force constant on the enzyme in order to restrict any drastic changes. MD simulations were performed via NPT (constant number of atoms, constant pressure i.e. 1.01325 bar and constant temperature i.e. 300 K) ensemble. The Nose-Hoover chain method was used as the default thermostat with 1.0 ps interval and Martyna-Tobias-Klein as the default barostat with 2.0 ps interval by applying isotropic coupling style. Long-range electrostatic forces were calculated based on Particle-mesh-based Ewald approach with the cut-off radius for coulombic forces set to 9.0 Å. Finally, the system subjected to produce MD simulations for 20 ns for protein-ligand complex. During the simulation every 1000 ps of the actual frame was stored. The dynamic behavior and structural changes of the systems were analyzed by the calculation of the root mean square deviation (RMSD) and RMSF. Subsequently, the energy-minimized structure calculated from the equilibrated trajectory system was evaluated for investigation of each ligand-protein complex interaction.

3.11. Prime MM-GBSA

The ligand binding energies (ΔG_{Bind}) were calculated for compound 80 and acarbose using Molecular mechanics/generalized born surface area (MM-GBSA) modules (Schrödinger LLC 2018) (75) based on the following equation;

$$\Delta G_{\text{Bind}} = E_{\text{Complex}} - [E_{\text{Receptor}} + E_{\text{Ligand}}]$$

Where ΔG_{Bind} is the calculated relative free energy which includes both ligand and receptor strain energy. E_{Complex} is the MM-GBSA energy of the minimized complex, and E_{Ligand} is the MM-GBSA energy of the ligand after removing it from the complex and allowing it to relax. E_{Receptor} is the MM-GBSA energy of relaxed protein after separating it from the ligand. The MM-GBSA calculation was performed based on the clustering method for energy calculation.

References

- [1] K. Wang, L. Bao, K. Ma, J. Zhang, B. Chen, J. Han, J. Ren, H. Luo, H. Liu, A novel class of α -glucosidase and HMG-CoA reductase inhibitors from *Ganoderma lucidum* contextum and the anti-diabetic properties of ganomycin I in KK-Ay mice, *European journal of medicinal chemistry* 127 (2017) 1035-1046.
- [2] V. Pogaku, K. Gangarapu, S. Basavoju, K.K. Tatapudi, S.B. Katragadda, Design, synthesis, molecular modelling, ADME prediction and anti-hyperglycemic evaluation of new pyrazole-triazolopyrimidine hybrids as potent α -glucosidase inhibitors. *Bioorganic chemistry* 93 (2019) 103307.
- [3] N. Kerru, A. Singh-Pillay, P. Awolarejo, Singh, Current anti-diabetic agents and their molecular targets: A review, *European journal of medicinal chemistry* 152 (2018) 436-488.
- [4] M. Taha, N.H. Ismail, S. Imran, A. Wadood, M. Ali, F. Rahim, A.A. Khan, M. Riaz, Novel thiosemicarbazide-oxadiazole hybrids as unprecedented inhibitors of yeast α -glucosidase and in silico binding analysis, *RSC advances* 6(40) (2016) 33733-33742.
- [5] U. Salar, M. Taha, K.M. Khan, N.H. Ismail, S. Imran, S. Perveen, S. Gul, A. Wadood, Syntheses of new 3-thiazolyl coumarin derivatives, in vitro α -glucosidase inhibitory activity, and molecular modeling studies, *European journal of medicinal chemistry* 122 (2016) 196-204.
- [6] H. Gao, Y.N. Huang, P.Y. Xu, J. Kawabata, Inhibitory effect on α -glucosidase by the fruits of *Terminalia chebula* Retz, *Food Chemistry* 105(2) (2007) 628-634.
- [7] M.H. Muskiet, L. Tonneijck, M.M. Smits, M.H. Kramer, H.J.L. Heerspink, D.H. van Raalte, Pleiotropic effects of type 2 diabetes management strategies on renal risk factors, *The lancet Diabetes & endocrinology* 3(5) (2015) 367-381.
- [8] K. Umanath, J.B. Lewis, Update on diabetic nephropathy: core curriculum 2018, *American Journal of Kidney Diseases* 71(6) (2018) 884-895.
- [9] H. Jayasekara, R.J. MacInnis, R. Room, D.R. English, Long-term alcohol consumption and breast, upper aero-digestive tract and colorectal cancer risk: a systematic review and meta-analysis, *Alcohol and alcoholism* 51(3) (2016) 315-330.
- [10] D.M. Parkin, L. Boyd, L. Walker, 16. The fraction of cancer attributable to lifestyle and environmental factors in the UK in 2010, *British journal of cancer* 105(S2) (2011) S77-S81.
- [11] R.A. Kowluru, M. Mishra, Oxidative stress, mitochondrial damage and diabetic retinopathy, *Biochimica et Biophysica Acta (BBA)-Molecular Basis of Disease* 1852(11) (2015) 2474-2483.

- [12] R. Chen, B. Ovbiagele, W. Feng, Diabetes and stroke: epidemiology, pathophysiology, pharmaceuticals and outcomes, *The American journal of the medical sciences* 351(4) (2016) 380-386.
- [13] M. Abdelsaid, R. Prakash, W. Li, M. Coucha, S. Hafez, M.H. Johnson, S.C. Fagan, A. Ergul, Metformin treatment in the period after stroke prevents nitrate stress and restores angiogenic signaling in the brain in diabetes, *Diabetes* 64(5) (2015) 1804-1817.
- [14] O. Hoffstad, N. Mitra, J. Walsh, D.J. Margolis, Diabetes, lower-extremity amputation, and death, *Diabetes care* 38(10) (2015) 1852-1857.
- [15] E.W. Gregg, N. Sattar, M.K. Ali, The changing face of diabetes complications, *The lancet Diabetes & endocrinology* 4(6) (2016) 537-547.
- [16] A.V. Haas, M.E. McDonnell, Pathogenesis of cardiovascular disease in diabetes, *Endocrinology and Metabolism Clinics* 47(1) (2018) 51-63.
- [17] F. Fiordaliso, G. Clerici, S. Maggioni, M. Caminiti, C. Bisighini, D. Novelli, D. Minnella, A. Corbelli, R. Morisi, A. De Iaco, Prospective study on microangiopathy in type 2 diabetic foot ulcer, *Diabetologia* 59(7) (2016) 1542-1548.
- [18] E. Rubinat, E. Ortega, A. Traveset, M.V. Arcidiacono, N. Alonso, A. Betriu, M. Granado-Casas, M. Hernández, J. Soldevila, M. Puig-Domingo, Microangiopathy of common carotid vasa vasorum in type 1 diabetes mellitus, *Atherosclerosis* 241(2) (2015) 334-338.
- [19] S.D. Doddaramappa, K.L. Rai, N. Srikantamurthy, J. Chetani, Novel 5-functionalized-pyrazoles: Synthesis, characterization and pharmacological screening, *Bioorganic & medicinal chemistry letters* 25(17) (2015) 3671-3675.
- [20] F.A. van de Laar, Alpha-glucosidase inhibitors in the early treatment of type 2 diabetes, *Vascular Health and Risk Management* 4(6) (2008) 1189-1195.
- [21] S. Hameed, F. Seraj, R. Rafique, S. Chigurupati, A. Madood, A.U. Rehman, V. Venugopal, U. Salar, M. Taha, K.M. Khan, Synthesis of benzotriazole derivatives and their dual potential as α -amylase and α -glucosidase inhibitors in vitro: Structure activity relationship, molecular docking, and kinetic studies, *European journal of medicinal chemistry* 183 (2019) 111677.
- [22] P. Singh, S. Mothilal, N. Kerru, A. Singh, M. Pillay, L. Gummidi, O.L. Erukainure, M.S. Islam, Comparative α -glucosidase and α -amylase inhibition studies of rhodanine-pyrazole conjugates and their simple rhodanine analogues, *Medicinal Chemistry Research* 28(2) (2019) 143-159.
- [23] N. Jong-Anurakkun, M.R. Bhandari, J. Kawabata, α -Glucosidase inhibitors from Devil tree (*Alstonia scholaris*), *Food Chemistry* 103(4) (2007) 1319-1323.
- [24] X. Wu, G. Zhang, M. Hu, L. Fan, A. Li, Y. Zhang, Molecular characteristics of gallic catechin gallate affecting protein glycation, *Food Hydrocolloids* 105 (2020) 105782.
- [25] S. Imran, M. Taha, N. Ismail, S.M. Kashif, F. Rahim, W. Jamil, M. Hariono, M. Yusuf, H. Wahab, Synthesis of novel flavone hydrazones: In-vitro evaluation of α -glucosidase inhibition, QSAR analysis and docking studies, *European journal of medicinal chemistry* 105 (2015) 156-170.
- [26] E. Simsek, X. Lu, S. Ouzounov, T.M. Block, A.S. Mehta, α -Glucosidase inhibitors have a prolonged antiviral effect against hepatitis B virus through the sustained inhibition of the large and middle envelope glycoproteins, *Antiviral Chemistry and Chemotherapy* 17(5) (2006) 259-267.
- [27] C. Durinx, A.M. Lambeir, E. Bosmans, J.B. Falmagne, R. Berghmans, A. Haemers, S. Scharpé, I. De Meester, Molecular characterization of dipeptidyl peptidase activity in serum: soluble CD26/dipeptidyl peptidase IV is responsible for the release of X-Pro dipeptides, *European Journal of Biochemistry* 267(17) (2000) 5608-5613.
- [28] J.W. Dennis, S. Laferte, C. Waghorne, M.L. Breitman, R.S. Kerbel, Beta 1-6 branching of Asn-linked oligosaccharides is directly associated with metastasis, *Science* 236(4801) (1987) 582-585.
- [29] G.S. Jacob, Glycosylation inhibitors in biology and medicine, *Current opinion in structural biology* 5(5) (1995) 605-611.

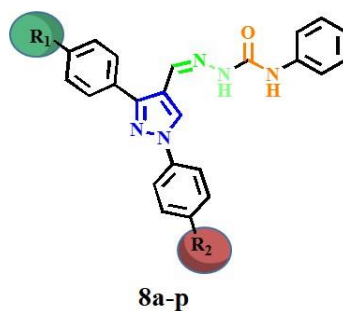
- [30] J.-F. Hsieh, W.-J. Lin, K.-F. Huang, J.-H. Liao, M.-J. Don, C.-C. Shen, Y.-J. Shiao, W.-T. Li, Antioxidant activity and inhibition of α -glucosidase by hydroxyl-functionalized 2-arylbenzo [b] furans, *European journal of medicinal chemistry* 93 (2015) 443-451.
- [31] E.A. Nyenwe, T.W. Jerkins, G.E. Umpierrez, A.E. Kitabchi, Management of type 2 diabetes: evolving strategies for the treatment of patients with type 2 diabetes, *Metabolism* 60(1) (2011) 1-23.
- [32] P. Hollander, Safety profile of acarbose, an α -glucosidase inhibitor, *Drugs* 44(3) (1992) 47-53.
- [33] S.-H. Park, J.-Y. Kim, J.-S. Kim, C. Jung, D.-K. Song, W.-H. Ham, 1, 3-Oxazine as a chiral building block used in the total synthesis of (+)-1-deoxynojirimycin and (2R, 5R)-dihydroxymethyl-(3R, 4R)-dihydroxypyrrolidine, *Tetrahedron: Asymmetry* 26(12-13) (2015) 657-661.
- [34] M.F. Khan, M.M. Alam, G. Verma, W. Akhtar, M. Akhter, M. Shaquiquzzaman, The therapeutic voyage of pyrazole and its analogs: a review, *European journal of medicinal chemistry* 120 (2016) 170-201.
- [35] M. Faisal, A. Saeed, S. Hussain, P. Dar, F.A. Larik, Recent developments in synthetic chemistry and biological activities of pyrazole derivatives, *Journal of Chemical Sciences* 131(8) (2019) 70.
- [36] P.A. Channar, A. Saeed, F.A. Larik, B. Batool, S. Kalsoom, M. Hasan, M.F. Erben, H.R. El-Seedi, M. Ali, Z. Ashraf, Synthesis of aryl pyrazole via Suzuki coupling reaction, in vitro mushroom tyrosinase enzyme inhibition assay and in silico comparative molecular docking analysis with Kojic acid, *Bioorganic chemistry* 79 (2018) 293-300.
- [37] F.E. Bennani, L. Doudach, Y. Cherrah, Y. Ramli, K. Karrouchi, M.E.A. Faouzi, Overview of recent developments of pyrazole derivatives as an anticancer agent in different cell line, *Bioorganic chemistry* 97 (2020) 103470.
- [38] P.A. Channar, S. Afzal, S.A. Ejaz, A. Saeed, F.A. Larik, F.A. Mahesar, J. Lecka, J. Sévigny, M.F. Erben, J. Iqbal, Exploration of carboxy pyrazole derivatives: Synthesis, alkaline phosphatase, nucleotide pyrophosphatase/phosphodiesterase and nucleoside triphosphate diphosphohydrolase inhibition studies with potential anticancer profile, *European journal of medicinal chemistry* 156 (2018) 461-478.
- [39] A.A. Estrada, B.K. Chan, C. Baker-Glen, A. Beresford, D.J. Burdick, M. Chambers, H. Chen, S.L. Dominguez, J. Dotson, J. Drummond, Discovery of highly potent, selective, and brain-penetrant aminopyrazole leucine-rich repeat kinase 2 (LRRK2) small molecule inhibitors, *Journal of medicinal chemistry* 57(3) (2014) 921-936.
- [40] D.L. Smith, A.A. Forist, W.F. Dulin, 5-Methylpyrazole-3-carboxylic acid. The potent hypoglycemic metabolite of 3, 5-dimethylpyrazole in the rat, *Journal of medicinal chemistry* 8(3) (1965) 350-353.
- [41] H.M. Faidallah, K.A. Khan, A.M. Asiri, Synthesis and biological evaluation of new 3-trifluoromethylpyrazole carbonyl urea and thiourea derivatives as antidiabetic and antimicrobial agents, *Journal of Fluorine Chemistry* 132(2) (2011) 131-137.
- [42] K. Rikimaru, T. Wakabayashi, H. Abe, H. Imoto, T. Maekawa, O. Ujikawa, K. Murase, T. Matsuo, M. Matsumoto, C. Nomura, A new class of non-thiazolidinedione, non-carboxylic-acid-based highly selective peroxisome proliferator-activated receptor (PPAR) γ agonists: design and synthesis of benzylpyrazole acylsulfonamides, *Bioorganic & medicinal chemistry* 20(2) (2012) 714-733.
- [43] D.-M. Shen, E.J. Brady, M.R. Candelore, Q. Dallas-Yang, V.D.-H. Ding, W.P. Feeney, G. Jiang, M.E. McCann, S. Mock, S.A. Qureshi, Discovery of novel, potent, selective, and orally active human glucagon receptor antagonists containing a pyrazole core, *Bioorganic & medicinal chemistry letters* 21(1) (2011) 76-81.
- [44] D.A. Griffith, R.L. Dow, K. Huard, D.J. Edmonds, S.W. Bagley, J. Polivkova, D. Zeng, C.N. Garcia-Irizarry, J.A. Southers, W. Esler, Spirolactam-based acetyl-CoA carboxylase inhibitors: toward improved metabolic stability of a chromanone lead structure, *Journal of medicinal chemistry* 56(17) (2013) 7110-7119.

- [45] K. Huard, S.W. Bagley, E. Menhaji-Klotz, C. Prévile, J.A. Southers Jr, A.C. Smith, D.J. Edmonds, J.C. Lucas, M.F. Dunn, N.M. Allanson, Synthesis of spiropiperidine lactam acetyl-CoA carboxylase inhibitors, *The Journal of Organic Chemistry* 77(22) (2012) 10050-10057.
- [46] E. Hernández-Vázquez, R. Aguayo-Ortiz, J.J. Ramírez-Espinosa, S. Estrada-Soto, F. Hernández-Luis, Synthesis, hypoglycemic activity and molecular modeling studies of pyrazole-3-carbohydrazides designed by a CoMFA model, *European journal of medicinal chemistry* 69 (2013) 10-21.
- [47] F. Peytam, M. Adib, R. Shourgeshty, M. Mohammadi-Khanaposhtani, M. Jahani, S. Imanparast, M.A. Faramarzi, M. Mahdavi, A.A. Moghadamnia, H. Rastegar, Design and synthesis of new imidazo [1, 2-b] pyrazole derivatives, in vitro α -glucosidase inhibition, kinetic and docking studies, *Molecular Diversity* 24(1) (2020) 69-80.
- [48] K.M. Khan, M. Irfan, M. Ashraf, M. Taha, S.M. Saad, S. Perveen, M.I. Choudhary, Synthesis of phenyl thiazole hydrazones and their activity against glycation of proteins, *Medicinal Chemistry Research* 24(7) (2015) 3077-3085.
- [49] K. Mohammed Khan, Z. Shah, V. Uddin Ahmad, M. Khan, M. Taha, F. Mahim, S. Ali, N. Ambreen, S. Perveen, M. Iqbal Choudhary, 2, 4, 6-Trichlorophenylhydrazine Schiff bases as DPPH radical and super oxide anion scavengers, *Medicinal Chemistry* 8(3) (2012) 452-461.
- [50] M. Taha, N.H. Ismail, M. Ali, K.M. Khan, W. Jamil, S.M. Kashif, M. Asraf, Synthesis of indole-2-hydrazones in search of potential leishmanicidal agents, *Medicinal Chemistry Research* 23(12) (2014) 5282-5293.
- [51] F.D. Popp, W. KIRSCH, Synthesis of potential anticancer agents. V. Schiff bases and related Compounds 1-2, *The Journal of Organic Chemistry* 26(10) (1961) 3858-3860.
- [52] S. Imran, M. Taha, N.H. Ismail, K.M. Khan, G. Noor, M. Hussain, S. Tauseef, Synthesis of novel bisindolylmethane Schiff bases and their antibacterial activity, *Molecules* 19(8) (2014) 11722-11740.
- [53] J.S. Jain, R.S. Srivastava, N. Aggarwal, P. Sinha, Synthesis and evaluation of Schiff bases for anticonvulsant and behavioral depressant properties, *Central Nervous System Agents in Medicinal Chemistry (Formerly Current Medicinal Chemistry-Central Nervous System Agents)* 7(3) (2007) 200-204.
- [54] M. Taha, N.H. Ismail, S. Lalani, M.C. Fatmi, S. Siddiqui, K.M. Khan, S. Imran, M.I. Choudhary, Synthesis of novel inhibitors of α -glucosidase based on the benzothiazole skeleton containing benzohydrazide moiety and their molecular docking studies, *European journal of medicinal chemistry* 92 (2015) 387-400.
- [55] M. Sherafati, M. Mohammadi-Khanaposhtani, S. Moradi, M.S. Asgari, N. Najafabadipour, M.A. Faramarzi, M. Mahdavi, M. Biglar, B. Larijani, H. Hamedifar, Design, synthesis and biological evaluation of novel phthalimide-Schiff base-coumarin hybrids as potent α -glucosidase inhibitors, *Chemical Papers* (2020) 1-10.
- [56] S.E. Sadat-Ebrahimi, A. Rahmani, M. Mohammadi-Khanaposhtani, S. Mojtavavi, M.A. Faramarzi, M. Emadi, A. Yahya-Meymandi, B. Larijani, M. Biglar, M. Mahdavi, New phthalimide-benzamide-1, 2, 3-triazole hybrids; design, synthesis, α -glucosidase inhibition assay, and docking study, *Medicinal Chemistry Research* (2020) 1-9.
- [57] M. Ali, K.M. Khan, M. Mahdavi, A. Jabbar, S. Shamim, U. Salar, M. Taha, S. Parveen, B. Larijani, M.A. Faramarzi, Synthesis, In vitro and In silico Screening of 2-Amino-4-Aryl-6-(phenylthio) pyridine-3, 5-dicarbonitriles as Novel α -Glucosidase Inhibitors, *Bioorganic chemistry* (2020) 103879.
- [58] Y. Liu, L. Ma, W.-H. Chen, B. Wang, Z.-L. Xu, Synthesis of xanthone derivatives with extended π -systems as α -glucosidase inhibitors: Insight into the probable binding mode, *Bioorganic & medicinal chemistry* 15(8) (2007) 2810-2814.
- [59] G.-L. Li, J.-Y. He, A. Zhang, Y. Wan, B. Wang, W.-H. Chen, Toward potent α -glucosidase inhibitors based on xanthenes: A closer look into the structure-activity correlations, *European journal of medicinal chemistry* 46(9) (2011) 4050-4055.

- [60] P. Yogeeswari, R. Thirumurugan, R. Kavya, J.S. Samuel, J. Stables, D. Sriram, 3-Chloro-2-methylphenyl-substituted semicarbazones: synthesis and anticonvulsant activity, *European journal of medicinal chemistry* 39(8) (2004) 729-734.
- [61] H.P. Singh, S. Pandeya, C. Chauhan, C.S. Sharma, Synthesis and pharmacological screening of some novel chalconyl derivatives of substituted phenyl semicarbazide, *Medicinal Chemistry Research* 20(1) (2011) 74-80.
- [62] T. Hsu, C.T. Chen, T.Y. Tsai, J.H. Cheng, S.Y. Wu, C.N. Chang, C.H. Chien, K.C. Yeh, Y.W. Huang, C.L. Huang, (1, 3-Diphenyl-1H-Pyrazol-4-yl)-Methylamine Analogues as Inhibitors of Dipeptidyl Peptidases, *Journal of the Chinese Chemical Society* 56(5) (2009) 1048-1055.
- [63] M.S. Asgari, M. Mohammadi-Khanaposhtani, M. Kiani, P.R. Ranjbar, E. Zabihi, R. Pourbagher, R. Rahimi, M.A. Faramarzi, M. Biglar, B. Larijani, Biscoumarin-1, 2, 3-triazole hybrids as novel anti-diabetic agents: Design, synthesis, in vitro α -glucosidase inhibition, kinetic, and docking studies, *Bioorganic chemistry* 92 (2019) 103206.
- [64] M. Saeedi, M. Mohammadi-Khanaposhtani, M.S. Asgari, N. Eghbali, S. Imanparast, M.A. Faramarzi, B. Larijani, M. Mahdavi, T. Akbarzadeh, Design, synthesis, in vitro, and in silico studies of novel diarylimidazole-1, 2, 3-triazole hybrids as potent α -glucosidase inhibitors, *Bioorganic & medicinal chemistry* 27(23) (2019) 115148.
- [65] H. Ding, X. Wu, J. Pan, X. Hu, D. Gong, G. Zhang, New insights into the inhibition mechanism of betulonic acid on α -glucosidase, *Journal of agricultural and food chemistry* 66(27) (2018) 7065-7075.
- [66] X. Peng, G. Zhang, Y. Liao, D. Gong, Inhibitory kinetics and mechanism of kaempferol on α -glucosidase, *Food Chemistry* 190 (2016) 207-215.
- [67] D. Shahzad, A. Saeed, F.A. Larik, P.A. Channar, Q. Abbas, M.F. Alajmi, M.I. Arshad, M.F. Erben, M. Hassan, H. Raza, Novel C-2 Symmetric Molecules as α -Glucosidase and α -Amylase Inhibitors: Design, Synthesis, Kinetic Evaluation, Molecular Docking and Pharmacokinetics, *Molecules* 24(8) (2019) 1511.
- [68] UniProt: the universal protein knowledgebase, *Nucleic acids research* 45(D1) (2017) D158-D169.
- [69] Y.H. Song, D.W. Kim, M.J. Curtis-Long, C. Park, M. Son, J.Y. Kim, H.J. Yuk, K.W. Lee, K.H. Park, Cinnamic acid amides from *Tribulus terrestris* displaying uncompetitive α -glucosidase inhibition, *European journal of medicinal chemistry* 114 (2016) 201-208.
- [70] K. Yamamoto, H. Miyake, M. Kusunoki, S. Osaki, Crystal structures of isomaltase from *Saccharomyces cerevisiae* and in complex with its competitive inhibitor maltose, *The FEBS journal* 277(20) (2010) 4205-4214.
- [71] S.N. Pandeya, P. Yogeeswari, J.P. Stables, Synthesis and anticonvulsant activity of 4-bromophenyl substituted aryl semicarbazones, *European journal of medicinal chemistry* 35(10) (2000) 879-886.
- [72] M. Adib, F. Peytam, M. Rahmanian-Jazi, S. Mahernia, H.R. Bijanzadeh, M. Jahani, M. Mohammadi-Khanaposhtani, S. Imanparast, M.A. Faramarzi, M. Mahdavi, New 6-amino-pyrido [2, 3-d] pyrimidine-2, 4-diones as novel agents to treat type 2 diabetes: A simple and efficient synthesis, α -glucosidase inhibition, molecular modeling and kinetic study, *European journal of medicinal chemistry* 155 (2018) 353-363.
- [73] S.C. Lovell, I.W. Davis, W.B. Arendall III, P.I. De Bakker, J.M. Word, M.G. Prisant, J.S. Richardson, D.C. Richardson, Structure validation by C α geometry: ϕ , ψ and C β deviation, *Proteins: Structure, Function, and Bioinformatics* 50(3) (2003) 437-450.
- [74] D. Eisenberg, R. Lüthy, J.U. Bowie, [20] VERIFY3D: assessment of protein models with three-dimensional profiles, *Methods in enzymology*, Elsevier 1997, pp. 396-404.
- [75] M. Wiederstein, M.J. Sippl, ProSA-web: interactive web service for the recognition of errors in three-dimensional structures of proteins, *Nucleic acids research* 35(suppl_2) (2007) W407-W410.
- [76] F. Azimi, J.B. Ghasemi, L. Saghaei, F. Hassanzadeh, M. Mahdavi, H. Sadeghi-Aliabadi, M.T. Scotti, L. Scotti, Identification of Essential 2D and 3D Chemical Features for Discovery of the Novel Tubulin Polymerization Inhibitors, *Current topics in medicinal chemistry* 19(13) (2019) 1092-1120.

[77] L. Schrödinger, Schrödinger Release 2015-4: Desmond molecular dynamics system, Maestro-Desmond interoperability tools, DE Shaw Research, Schrödinger, New York, NY (2015).

Journal Pre-proof

Table 1In vitro α -glucosidase inhibitory activity of compounds 8a-p.

Compound	R ₁	R ₂	IC ₅₀ (μ M) ^a
8a	H	H	96.3 \pm 0.8
8b	CH ₃	H	157.3 \pm 1.9
8c	OCH ₃	H	182.6 \pm 2.3
8d	Cl	H	159 \pm 1.7
8e	Br	H	160.2 \pm 2.0
8f	NO ₂	H	130.7 \pm 1.5
8g	OH	H	134.5 \pm 1.6
8h	F	H	695.0 \pm 9.5
8i	CF ₃	H	92.0 \pm 0.7
8j	H	CH ₃	387.7 \pm 5.0
8k	CH ₃	CH ₃	77.0 \pm 0.5
8l	OCH ₃	CH ₃	89.6 \pm 0.7
8m	Cl	CH ₃	116.7 \pm 1.3
8n	Br	CH ₃	506.2 \pm 8.5
8o	NO ₂	CH ₃	65.1 \pm 0.3
8p	OH	CH ₃	86.3 \pm 0.6
acarbose	-	-	750.0 \pm 10.0

^a Values are the mean \pm SD. All experiments were performed at least three times.

Table 2

Cytotoxicity of the most potent compounds 8o, 8k, 8p, 8l, 8i and 8a against 3T3 cell line.

Compounds	Cytotoxicity (3T3 cell line) IC ₅₀ (μM) ^a
8o	>50
8k	>50
8p	>50
8l	>50
8i	>50
8a	>50

^a All experiments were performed at least three times.

Fig. 1. Pyrazole derivatives as antidiabetic and hypoglycemic agents

Fig. 2. Rational design of new pyrazole-phenyl semicarbazone hybrids as potent α -glucosidase inhibitors based on molecular hybridization of pharmacophore units. (A-C) potent reported antidiabetic agent. (D) phenyl semicarbazide as modified pharmacophore of benzohydrazide. (E) Predicted interactions of the designed hybrid with a glucosidase. The green dashed lines stand for hydrogen bonds.

Scheme 1. Synthetic pathway of pyrazole-phenyl semicarbazone hybrids (8a-p)

Fig. 3. Kinetic study of α -glucosidase inhibition by compound 8o. (a) The Lineweaver–Burk plot in the absence and presence of different concentrations of compound 8o (μM); (b) the secondary plot between $1/V_{\text{max}}$ and various concentrations of compound 8o.

Fig. 4. (a) 3D-structural model of *S. cerevisiae* α -glucosidase bound to acarbose. The predicted binding modes of (b) acarbose, (c) compound 8o, (d) compound 8k, (e) compound 8p and compound 8l and (f) compound 8i, in the active site pocket. Residues that may be involved in the interactions of compound binding are drawn with stick model and shown in different colors. The possible hydrogen-bond interactions are indicated with dashed lines (green).

Fig. 5. RMSF plot of the α -glycosidase $\text{C}\alpha$ in complexed with compound 8o (in yellow) and acarbose (in green) for over 20 ns MD simulation time (b).

Fig. 6. shows the detailed orientation and ligand atom interactions that occurred more than 30.0% of the simulation time during the equilibrated phase over α -glycosidase complexed with compound 8o (a, b) and acarbose (c, d). Domain A, domain B and the flap region covered the mouth of the active site colored in yellow, blue and pink, respectively.

Author Statement

Fateme Azimi: Investigation, Conceptualization, Methodology, Validation, Writing - Original Draft

Jahan B. Ghasemi: Software

Homa Azizian: Software, Methodology

Mohammad Najafi: Software, Writing - Review & Editing

Mohammad Ali Faramarzi: Resources

Lotfollah Saghaei: Conceptualization, Project administration

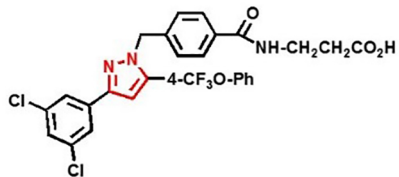
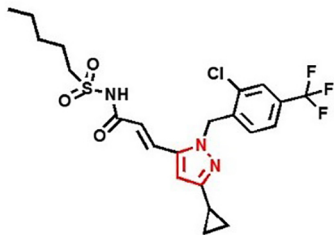
Hojjat Sadeghi-aliabadi: Resources

Bagher Larijani: Funding acquisition,

Farshid Hassanzadeh: Project administration, Conceptualization

Mohammad Mahdavi: Conceptualization, Project administration

Antidiabetic agents



Hypoglycemic agents

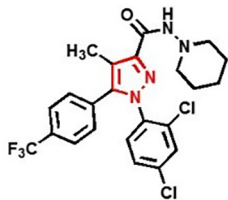
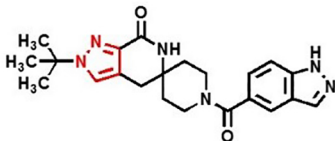
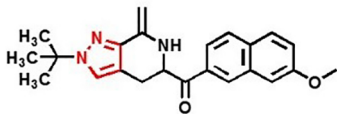
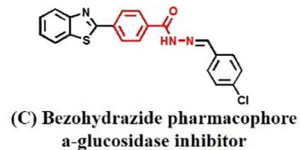
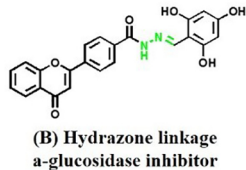
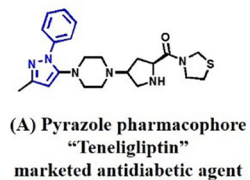


Figure 1



Modification

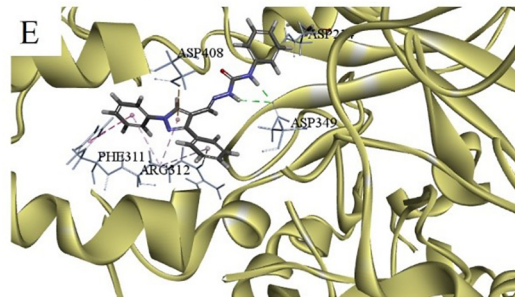
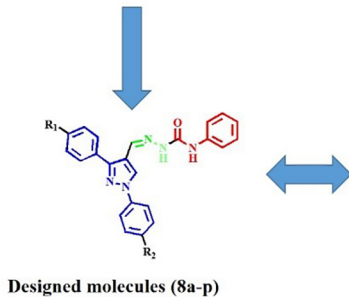
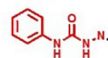


Figure 2

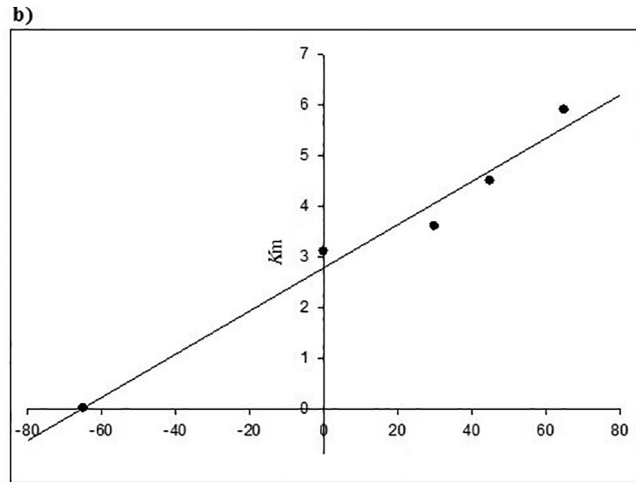
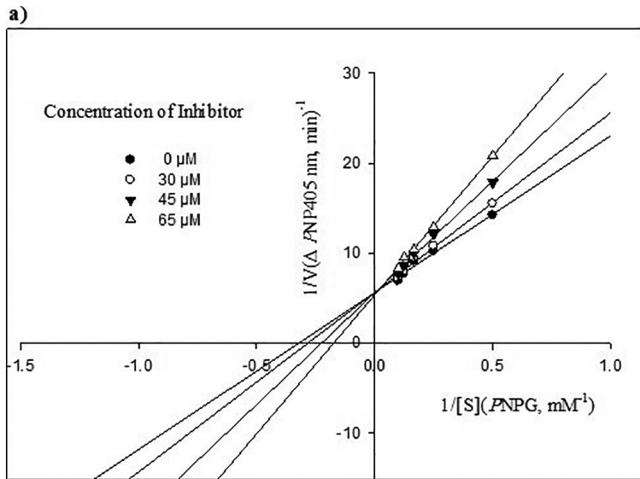


Figure 3

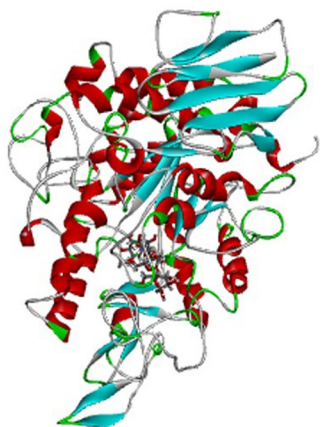
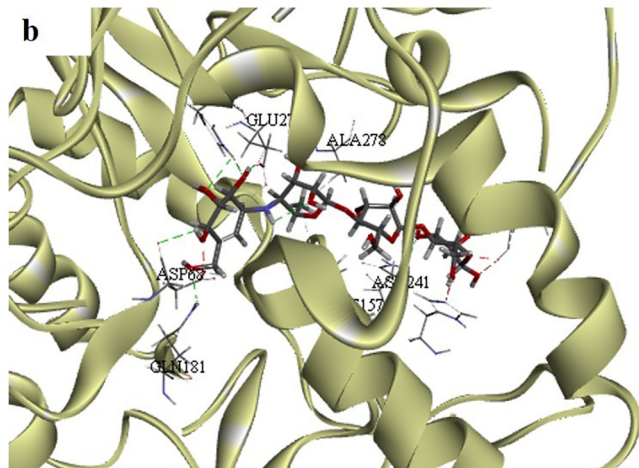
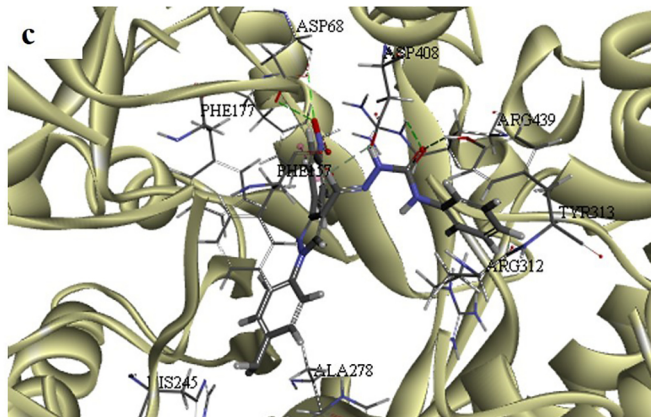
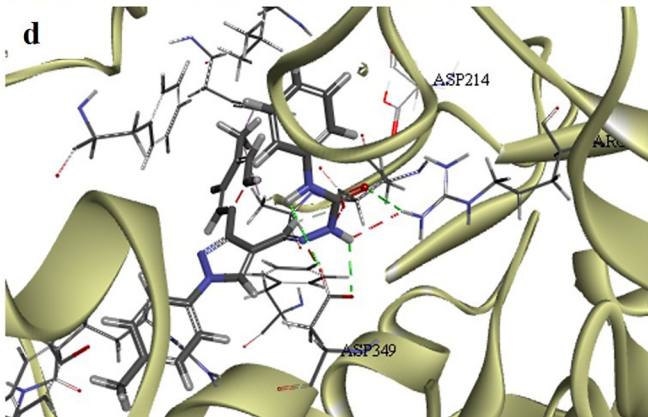
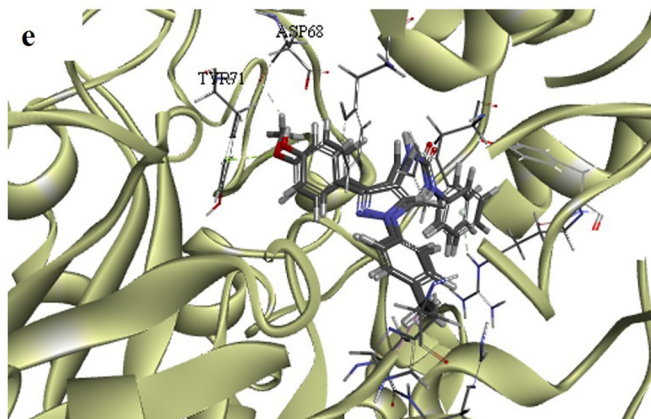
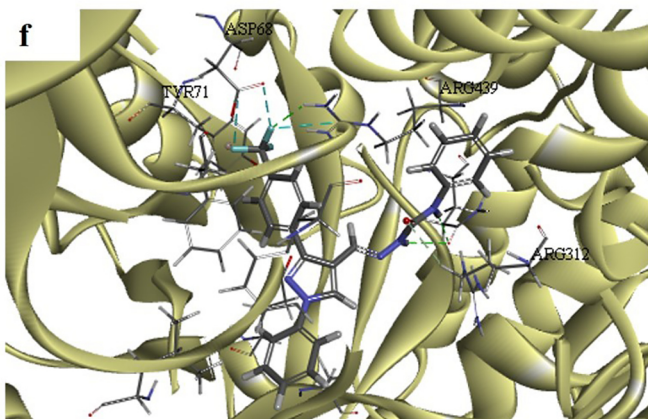
a**b****c****d****e****f**

Figure 4

RMSF Plot

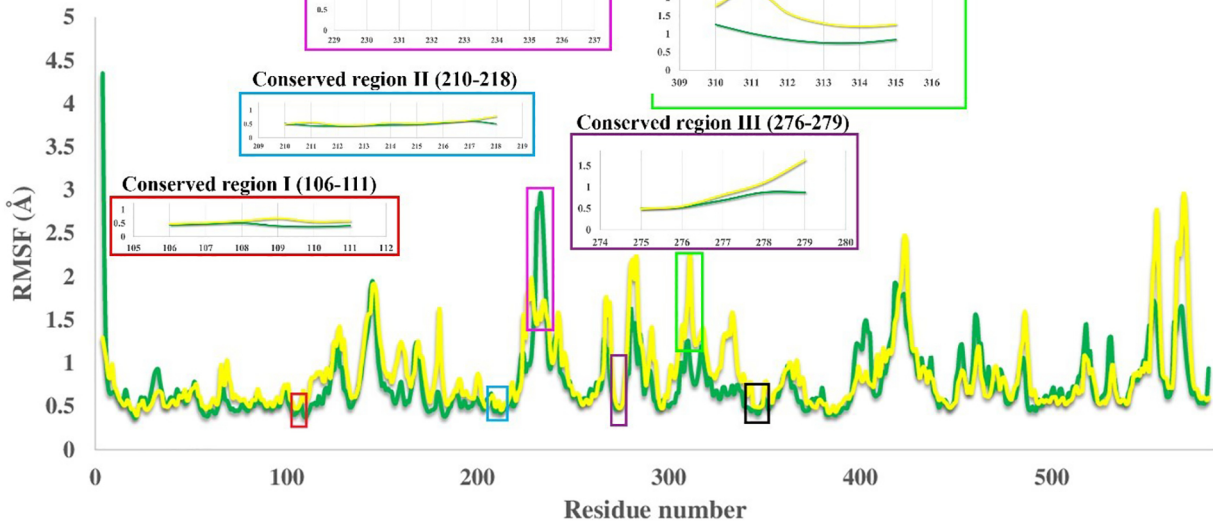


Figure 5

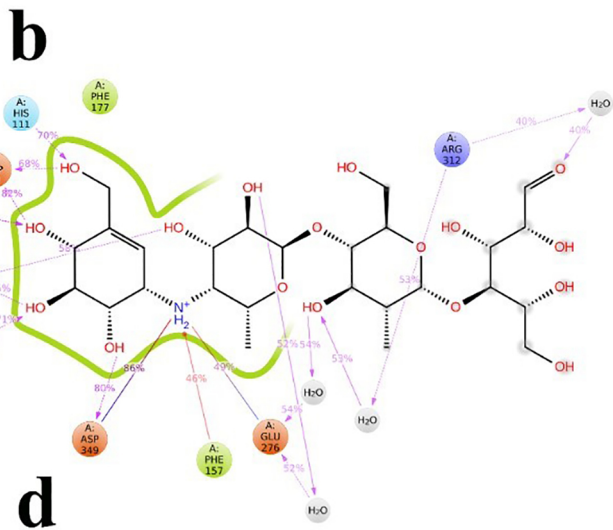
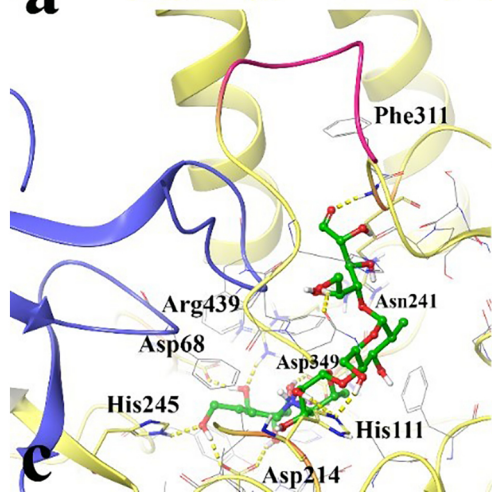
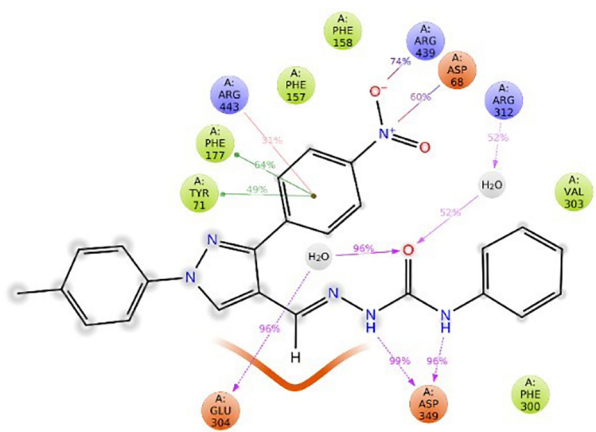
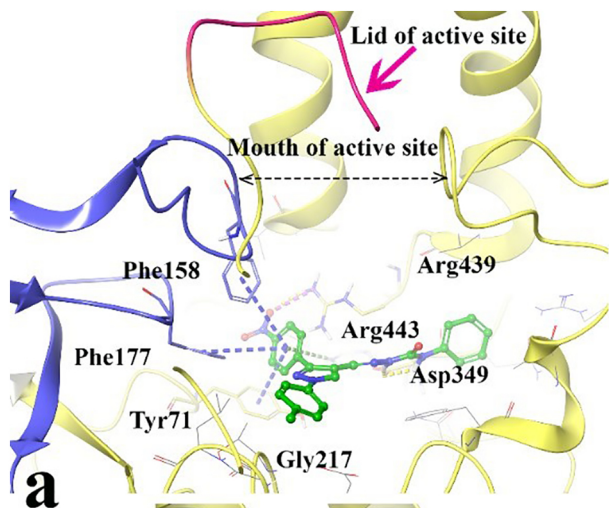


Figure 6